Politecnico di Torino

College of Computer Engineering, Cinema and Mechatronics

Master's Degree in Mechatronic Engineering

Master's Degree Thesis

Advances in the Development of a Spherical Rover for
Planetary Exploration - Part 2 : Modelling and Control

Supervisor: **Candidate:**

Prof. Stefano MAURO   Paolo GUALBERTO

Dr. Matteo MELCHIORRE

Academic year 2023 - 2024

Abstract

In the following, an introductory summary of previous work is presented. Given the complete design of the robot, it is possible to proceed with the functional and performance study, both in terms of motor capabilities and electronic efficiency, considering multiple scenarios. The appropriate sizing of the internal battery is calculated in order to continuously power the entire system for one hour. The robot is modeled in a multi-body simulation environment using Simulink/Simscape, replicating the entire plant system, including the precise internal mechanisms. Different versions of the plant have been developed. A first one consider every single components, inertia and relative motion among them. A second compact form version ,by simplifying the redundant connections, presents an analogous behavior as the first one and it is used for further analysis. The last version presents a simple shape made by connecting macro-group-components, and is used for studying the motion of the robot in real-time simulation. A beginning set of tests simulate the plant over different surfaces, in particular when the terrain is only uphill, only downhill or has sinusoidal shape. The tests present an open loop system where the robot behavior has been analyzed either putting a constant reference from simulink, or connecting a joystick device via USB port. Therefore, starting from the aforementioned plant system, the thesis proposes the development of a corresponding closed loop controller system capable of maneuvering the spherical ROV. Given a linear speed input the robot can be controlled along a straight path, and follows curved trajectories by auxiliary imposing the pendulum angle during lateral oscillation. Every virtual data input to the controller is sourced from a sensor previously defined and implemented into the simulation. The controller development features a multi-closed-loop structure, consisting of PID controllers and saturation blocks. The results obtained from the Model-in-the-Loop (MiL) tests demonstrate optimal speed control during longitudinal

trajectories, strongly reducing the internal mechanism oscillations. Furthermore, the controller efficiently maneuvers the robot through movements on the plane in real time.

Contents

List of Tables

List of Figures

List of Abbreviations

ROV   Remotely Operated Vehicle

UGV   Unmanned Ground Vehicle

SAR   Search and Rescue

SMR   Spherical Mobile Robots

BCO   Barycenter Offset

BSR   Barycenter Spherical Robot

SR   Spherical Robot

IDU   Internal Driving Unit

PID   Propotional-Integrative-Derivative

DOF   Degrees of Freedom

CMG   Control Moment Gyroscope

COAM   Conservation of Angular Momentum

DC   Direct Current

RW   Reaction Wheel

LQR   Linear Quadratic Regulator

SUR   Spherical Underwater Robot

IMU   Inertial Measurement Unit

SIL   Software-in-the-Loop

MCU   MicroController Unit

COM   Center of Mass

SW   SolidWorks

SPI   Serial Peripheral Interface

Chapter 1

Introduction

The master's thesis discussed, presents the design of a spherical Rover. The project was proposed by Prof. Mauro of Dimeas Department of Politecnico di Torino, supervised by Prof. Mauro and Dr. M.Melchiorre.

Spherical robots (SRs) are of significant importance within the context of mobile robotics, offering several advantages over traditional mobile robot. Their geometry prevents them from tipping over and provides high resistance from impacts. Furthermore, the shell protects the internal components from contaminations and other possible environmental danger. The symmetrical design always allows the rover to regain control and to actuate fluid and responsive movements. Another important feature that characterises them is the energy saving in case of downhill movements. Furthermore, depending on their drive mechanisms, some SRs can achieve omnidirectional movement.

For the reasons listed above, spherical rovers represent a class with great technological and applicative potential. Being resistant to contamination and impact allows their use in search and rescue operations. Their robustness facilitates surveillance operations in difficult-to-access territories. Specific categories of Spherical Rovers are employed to use in underwater environments, as their shape allows them to be highly resistant to pressure. Several applications have been developed for data collection, environment monitoring and surveillance. Finally, they can be of considerable contribution to the branch of space exploration. Recent space programmes for the Moon and Mars have

led to an increase in the interest of space companies in such technologies.

Although the geometry is a distinctive feature, spherical rovers can be divided into multiple categories. The main difference that characterises them is the actuation of motion. Among the most well-known examples are hamsterballs, which feature an internal counterweight by which motion is generated. Fundamental differences between the categories are in their performance. Hamsterballs present themselves as rovers that are easier to control than pendulum-driven. However, the second ones are more effective for a wide variety of situations. This sector is therefore characterised by different approaches depending on the objectives to be achieved by the project.

In the thesis work, advances concerning the design and control system of a spherical rover are presented. The project examined is based on the work from M. Melchiorre and T. Colamartino. In the study by M. Melchiorre et al., the development of an Unmanned Ground Vehicle (UGV) [1] was addressed. Through a trade-off analysis, the project developed led to the definition of a prototype spherical rover with barycenter offset propulsion. The motion transmission principle and the main structure of the rover were defined. In particular, the pendulum has two degrees of freedom, enabling the rover to navigate curved trajectories. Kinematic of the differential system and dynamic formulas of the shell were defined and a control system was constructed to manoeuvre the rover.

Finally, the project objective were defined as follows:

Max. Step Height	$25mm$
Max. Slope Angle	$15°$
Min. Velocity	$2.5m/s$
Min. Acceleration	$0.5m/s^2$
Max Diameter	$0.5m$
Max Mass	$25kg$

Table 1.1: Design objective of [1].

Although the design performed well for control, the structure had some limitations for versatility and efficiency. One of the main points was the inability to achieve high torque values for overcoming obstacles.

The work carried out by T. Colamartino resulted in significant contributions in the

design and control management of the rover.A particular contribution can be found in the integration of two Control Moment Gyroscope (CMG), through which the slope climbing and the obstacle overcoming capabilities were increased. Through the principle of gyroscopic moment conservation, it is possible to provide a boost to the torque acting on the shell for overcoming steps up to $10cm$ in height. The equations linking gyroscopic actuation to obstacle overcoming have been derived and the main actuation components have been dimensioned.

Based on the 2D equations of dynamics, C. Colamartino developed a control system to manage straight motion. By implementing a Fuzzy Propotional-Integrative-Derivative (PID) control, the rover is able to faithfully follow speed profiles. Tests were carried out for step climbing too.
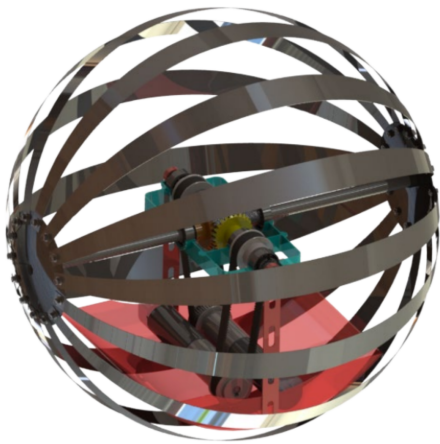
Figure 1.1: SR designed by M. Melchiorre.

Figure 1.2: SR designed by C. Colamartino.

This work presents the advances developed based on the design elaborated by Tommaso [2]. Although the rover had a well-defined design, no considerations were made from a constructional point of view.

The advances obtained as a result of the thesis have been divided into two parts. The first part aims at explaining the considerations regarding the final elaborated design, which is suitable for prototypation. Studies on weight, overall dimensions and internal force distribution were carried out. Electronic selections is addressed,

by considering the required measures and actuation needed for an effective control strategy.

This second part focuses on the performance analysis and the required power supply. Then, advances obtained with respect to the modelling of the plant and the development of planar control systems to manage the rover motion are reported.

1.1   Project Objectives

The aim of the thesis was to refine the components that make up the structure of the rover in detail, to guarantee operability without damage. The previous project presented a design conception and components positioning. However, the resulting design and performance assumptions, need to be coincident with physical structural limitations of the rover. Since the performance of the rover depends on the weight distribution and thus the geometry of the structure, it was necessary to identify the main points to achieve a trade-off between operability and feasibility of the supporting structure.

The final system must be able to acquire position and speed information to implement control strategy. Ideally, the objective is to derive an autonomous driving Rover. A major limitation of the design is the large amount of unusable space. In fact, since the pendulum structure is in constant rotation relative to the shell, the positioning of additional components is challenging. Choices must also be made in order to maintain high energy efficiency while keeping the centre of gravity of the system as low as possible to ensure that obstacles can be overcome.

Developing a control system that can manoeuvre the rover in planar space is a key objective. Since the rover is equipped with a 2-Degrees of Freedom (DOF) pendulum, it is necessary to implement a lateral angle control in order to define curvilinear trajectories. The presence of a forward position control only does not allow to fully implement the rover capabilities.

1.2 Contribution of this work

The thesis work presents a major contribution to the development and realisation of a prototypable model of a SR 2-DOF pendulum driven and the implementation of different control strategies. Work contributions can be resumed as follows:

- Comprehensive state-of-art to indviduate the fundamentals of the proposed work

- Design review. Identification of the system's failure points and dimensioning that takes into account the various working states of the system. Modifications must take into account the positioning of the centre of mass so as not to alter the performance of the system. The work can be considered as an estimate for production. Electronic components were defined for the implementation of a control system. In addition, the layout was chosen so that the movement of the various internal components would not be obstructed.

- Development of a 3D analytical model using Euler-Lagrange equations

- Development of a lateral model capable of exploiting the second degree of freedom. Subsequently, integration of the lateral control to the forward control for complete rover motion management. Different control algorithms were developed to test performances in several situations. Comparisons between management by separate and merged controls are rare in the literature, this work explores the possible cases.

The presented study is the result of a larger thesis project. Design aspects that have been anticipated are in Part 1. Developments concerning the performance analyisys,modelling and control of the rover are covered in this work.

Chapter 2

Resume of the Part 1

As mentioned in the introduction , the study performed in the thesis has been divided into two distinct parts. This chapter of thesis provides a summary of the topics covered in the previous subdivision including the obtained results.

In Part 1, the main topic is about the definition of the characteristics and the components that have been achieved in the final design of the rover. Firstly, a comprehensive state-of-art is presented to introduce the work by showing the main characteristics of the main Spherical Robot (SR) implemented technologies. Then, the previous work inhered from M. Melchiorre [1] and T. Colamartino [2] is shown in detail. Main formulas are presented in order to derive the considerations for the dimensioning of the components. The core of the previous work are the desctiption and selection of the electronic components and the sizing of the main components, in order to withstand the maximum load conditions.

2.1 Previous work

This project starts from the past considerations and models that M. Melchiorre and T. Colamartino have been derived. Through a trade-off, it was decided that pendulum driven spherical rovers are best compromise for their path accuracy and control simplicity. Then, CMGs have been introduced into the design to improve obstacle overcoming. The final result is a rover projected to climb steps of $10cm$-heigh and navigate in slope of 15°.

2.1.1 Melchiorre's thesis

In this thesis, the morphology of the pendulum and the design intent were defined. The resulting mechanism represents is a mechanic differential system located in the center of the sphere. Motion is generated by motors at the base of the pendulum and is transmitted to the side shafts of the differential by a system of belts and pulleys. Finally, the motion is distributed to the sphere according to the following kinematic formulas:

$$\omega_{pendulum} + \omega_{sphere} = \frac{\omega_{shaft_1} + \omega_{shaft_2}}{2} \tag{2.1}$$

$$\Omega_{pendulum} + \Omega_{sphere} = \frac{w_{shaft_1} + w_{shaft_2}}{2} \tag{2.2}$$

Finally, tests demonstrated the maneuverability of the rover. The derivation of an analytical model and a simplified simscape model made it possible to predict the rover's performance in different situations and ability to follow desired paths.

2.1.2 Colamartino's thesis

In this work, what was covered in the previous work was taken up and enriched with the addition of CMG systems. In this way, a lowering and weighting of the center of mass was achieved so as to ensure the possibility of overcoming larger obstacles. In addition, through the implementation of gyroscopes,it was defined a new step height possible to overcome.
Important contribution made was the development of a Fuzzy PID controller model by which it is possible to command the rover in forward path. The results showed great responsiveness and adaptation of the model to the reference values. The velocity profiles tested were both step and ramp.

2.2 Design review

The review consists of two main parts. The first focuses on defining the schematic of the electronics, such that the desired control can be implemented. The second part

involves sizing the structural parts so that they are not damaged during maximum load operations.

2.2.1 Electronics

From the control models, it is possible to deduce which sensors and actuators are the main ones to enable a reliable control system .

Motors

Motors are the basis of actuation. They are responsible for generating sufficient torque and speed to ensure the main motion and operation of the gyroscope systems. The selected motors are:

- Maxon RE 40 pendulum motors
- Maxon DCX 35 L spinning motors
- Nema 17 tilting stepper motors

Performances were evaluated and in order that the Rover could achieve the desired operating points. Stepper motors must be constantly powered since the tight space did not allow for a brake to be fitted.

Driver

These are components that act as an intermediary between the microcontroller and the motor. They allow the microcontroller to define the desired speed value by regulating the current input to the motor. They present systems to safeguard the motor with regard to the current supplying them. The drivers chosen are:

- ESCON 50/5 pendulum motor drivers
- BTS7960 spinning motor drivers
- TMC2208 tilting stepper motor drivers

Encoder

Encoders allow to measured the speed and position of the motor shaft. Speed measure is crucial regarding to pendulum motors, since they are used to keep the direction of the sphere and its speed as close as possible to the provided input. For stepper motors, position is also important since motors they are constantly active to keep the gyroscopes on axis. In fact, it is through the position signal, that we can force them to stay still and thus not be subject to oscillation. No encoders have been provided for spinning motors since an open-loop control is sufficient given the speed profile they must follow.

Selected components are:

- HEDL pendulum motor encoders

- AS5600 stepper motor encoders

IMU sensors

IMU sensors are used for the acquisition of angular speed and acceleration data. By integrating the given angular velocity it is also possible to estimate the pendulum angular position. Two IMU are implemented, one attached to the pendulum and the other one to the mechanic differential system.

NRF24L01

Joypad control has been thought to provide inputs from user. To implement this type of control, a transceiver is needed to communicate with the microcontroller and indicate input signals

Micro-controller

Arduino Mega Rev3 was chosen for the extensive documentation that allows faster implementation of the control system. It has the sufficient number of pins, and has good computational speed characteristics for what is needed

2.2.2 Final electronics design

Electronics connections are summarized in the picture below:

Figure 2.1: Scheme of the electronic network.

2.2.3   Mechanics

The mechanical structures was then discussed. The objective was to ensure the strength of the structure under the loads of the maximum acting torque. The sizing had to take into account the action of the gyroscopes

Main shaft

It is the main shaft of the pendulum. It must be able to withstand the maximum stress. The diameter selected is 15cm.

Cross joint

These are the joints between the shaft and ball. They are provided in aluminum

CMG

The CAD of the new parts compared with the previous versions and the new CMG unit are presented below:
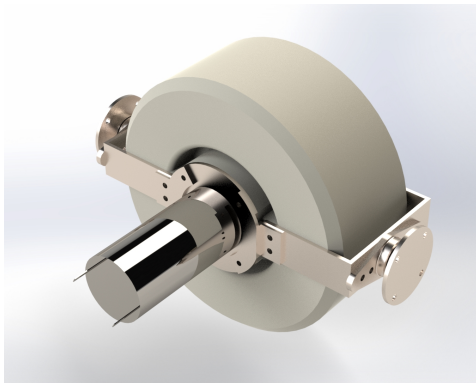
Figure 2.2: Initial CMG design.
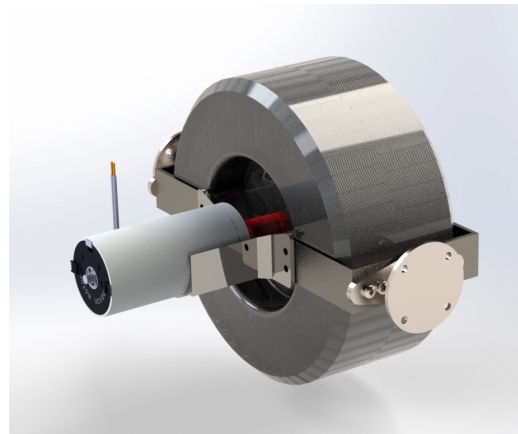
Figure 2.3: Final CMG design.

Main pendulum plate

Main pendulum plates allow the junction between mechanics differential system and the internal pendulum components, as it is one of the most important structural component of the design, this element was studied with a FEM analysis in order to demostrate the load resistance

Connection plate

Connection plate allows the junction between CMG group and the Main pendulum plate, FEM analysis is also made for this component

2.2.4 Final design

The final result of this chapter is a complete conception of the Spherical Rover. An emblematic figure that shows the entire design is presented in fig.2.4.
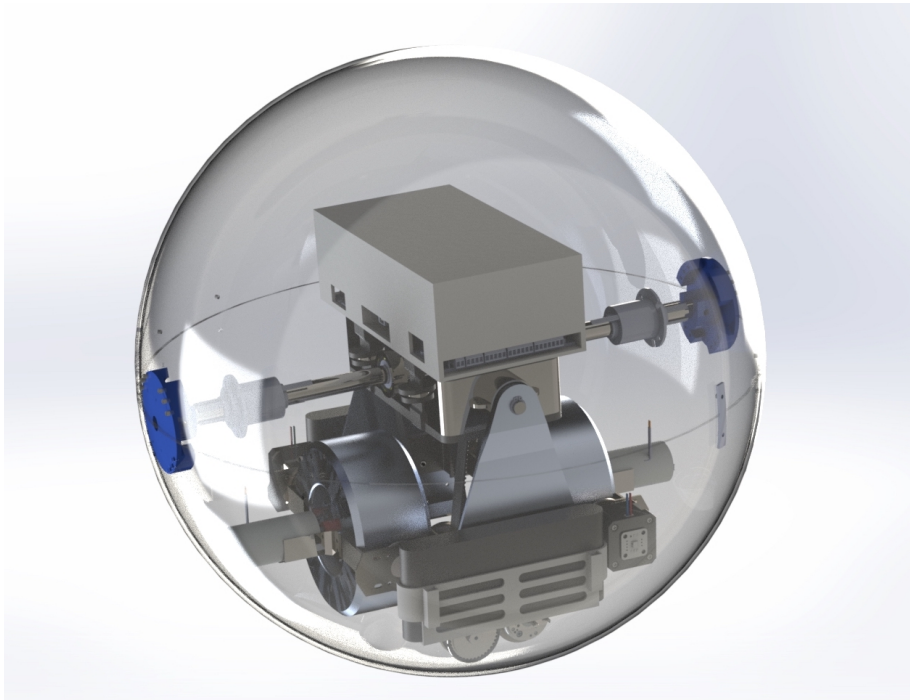
Figure 2.4: Final design of the spherical rover.

Chapter 3

Performance Analysis

3.1 Introduction

This chapter discusses the conditions of the main operating states of the rover. Starting from the considerations of the constraint reactions, it is possible to derive the effort required to maintain the pendulum at a desired inclination. Knowing also the sphere's forward velocity, it is possible to figure out the working point of the system. Consequently, the load situations of the motors can be deduced. A detailed analysis was carried out in the implementation of the CMGs.

As a result of this study, the considerations for the power supply were drawn up. By knowing the output power of a motor, it is possible to trace the electrical input power. The values obtained respect the motor's endurance limits for continuous power supply. The total consumption of the robot was evaluated as a weighted average of the expected situations combined with the ability to perform a certain number of steps. The choice of batteries was made taking into account the weight and bulk on the pendulum.

3.2 Rover characteristics and expected goals

The following tables lists the values obtained from the design section:

ROVER DATA		
M_S	$6.74kg$	Shell + differential system + electronics mass
m_P	$15.65kg$	Pendulum mass
a	$9.14cm$	Barycenter position of the SR
L_P	$13.57Nm$	Barycenter position of the pendulum
COEFFICIENTS		
η_D	0.98	Differential box efficiency
η_B	0.95	Belt efficiency
η_G	0.72	Gearhead efficiency
η_M	0.91	Pendulum motor efficiency
PENDULUM MOTOR DATA		
k_T	$30.2\,{}^{mNm}/_A$	Torque constant
k_V	$317\,{}^{rpm}/_V$	Speed constant
R_a	0.299Ω	Terminal resistance
GOALS		
R_S	$25cm$	Radio of the sphere
h	$10cm$	Maximum height of the step
ω	$10rad/s$	Nominal angular speed
α	$15°$	Nominal angle of the slope
T	$1h$	Operation time in nominal conditions

Table 3.1: Data of the final design and goals of the project. Motor and gearhead values are taken from datasheet [3] [4].

An important value to consider is the ratio $^a/_R$. Considering the model in the previous chapter, it is possible to calculate the new value of this ratio. This factor is important because it plays a fundamental role on the rover's performance. Indeed, having a lower centre of mass allows the rover to overcome higher steps without the activation of the CMGs.

Knowing the centre of mass of the system and the radius of the sphere, it is possible to compute the height of the maximum step that can be climbed. In [2] the relation

is derived as ratio between step height h and sphere radius R:

$$\frac{h}{R} = 1 - \sqrt{1 - \left(\frac{a + \frac{\tau_G}{(m_P + M_S)\,g}}{R}\right)} \qquad (3.1)$$

This implies that the use of CMGs is less required for overcoming obstacles. In the following paragraphs, it is shown how the activation of the gyroscopic manoeuvre requires a significant amount of energy. This is due to the preparation time for reaching spinning speed and the significant torques required from the main motors.

The pendulum's second degree of freedom can be neglected in the calculation of consumption. The tilting angle is limited from the presence of the main shaft. This implies that it is not possible to have a constant lateral acceleration. Thus, for a general application the major consumption of energy is caused by the forward acceleration.
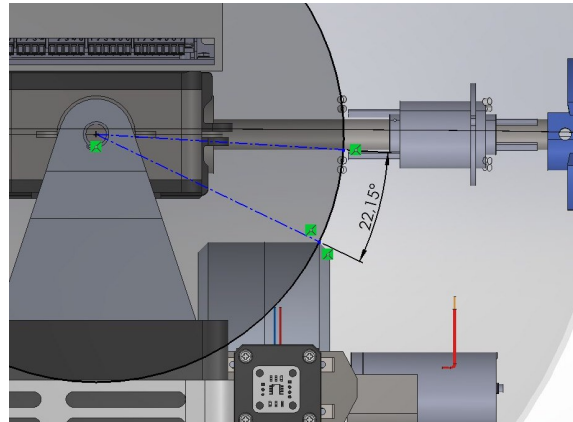
Figure 3.1: Maximum lateral angle.

The initial objective for the modelling was to have 1h operation under nominal conditions. However, it was pointed out that this condition could be too restrictive for modelling the rover. The followed approach in this work is to consider other scenarios for dimension the power supply, as advancing on the plain and repeated use of the gyroscopic manoeuvre. The final estimate obtained provides a more plausible prediction of the duration for continuous operation of the system.

3.3 Moving on a plain

The main requirement for this working point is to achieve a nominal speed of $2.5m/s$, i.e. a rolling speed of $10rad/s$. This condition is the starting point for determining the required motor speeds.

To determine the torque required to apply on the shell, the dissipative forces that would lead to deceleration must be identified. Considering the dissipative forces allows to identify the forward angle of the pendulum. From the angle of the pendulum, it is possible to determine the torque required by the motors.
For the pure rolling condition, the static friction force does not lead to a traceable consumption of the ball's kinetic energy. The forces that allow dissipation are rolling friction and viscous forces with air. Therefore, it is not possible to determine a general method for considering the friction forces acting on the shell as they are dependent on variable environmental factors. It was decided to impose an angle $\theta = 15°$ in order to account possible external forces.
The operative condition is computed as

$$\tau_P = l_P \, m_P \, g \, sin(\theta) \tag{3.2}$$

since the rolling speed is known, the required power is computed as

$$P_P = \tau_P \, \omega_P \tag{3.3}$$

The transmission system causes energy losses. These losses can be taken into account by dividing the final power requirement by the efficiency coefficients of the differential box, belts and gearheads. Finally, by dividing by two, the output power of a single motor is obtained:

$$P_M = \frac{P_P}{2 \cdot \eta_D \, \eta_B \, \eta_G} \tag{3.4}$$

Transmission takes place at a constant speed of $10rpm$. The selected gearheads have a gear ratio of 81:1, so the required motor speed is $7735rpm$. The useful output torque of the motor can be obtained by dividing the power by the rotational speed. The efficiency of the motor must be included in the calculation to find the required

input power. The effective torque of the motor is

$$\tau_M = \frac{P_M}{\eta_M \, \omega_M} \tag{3.5}$$

From there, values of current and voltage required can be computed as

$$\begin{cases} I = \frac{\tau_M}{k_T} \\ V = \frac{\omega_M}{k_V} + R_a \cdot I \end{cases} \tag{3.6}$$

k_T and k_V are the motor constants. Values and results are listed in the following table:

DATA		
θ	15°	Pendulum imposed angle
ω	$10^{rad}/s$	Sphere desired velocity
RESULTS		
I	$1.80A$	Motor required current
V	$24.89V$	Motor required voltage

Table 3.2: Data and results of main pendulum motors for planar trajectories.

3.4   Climbing a 15° slope

To achieve a constant speed, the sum of the forces acting on the rover must be equal to zero. When climbing an inclined plane, the gravitational force has a component parallel to the plane, which results in a negative acceleration. This force translates into a torque applied to the sphere. To balance this effect, the necessary moment must be computed and applied by tilting the pendulum. The pendulum must tilt so that the system's center of mass aligns with the contact point.
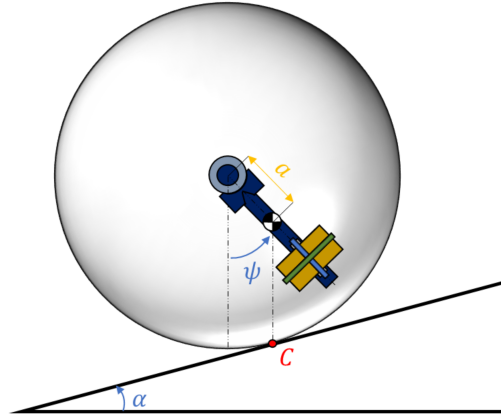
Figure 3.2: Equilibrium condition for the rover when climbing a slope.

Pendulum angle is computed as

$$\theta_{eq} = asin\left(\frac{R_S}{a}\,sin(\alpha)\right) \tag{3.7}$$

From here it is possible to compute the desired torque. It was decided to adopt a conservative approach by increasing the torque required at the pendulum by a factor η_{fr}. The final

$$\tau_P = \eta_{fr} \cdot l_P\, m_P\, g\, sin(\theta_{eq}) \tag{3.8}$$

Rotational speed is $\omega = 10rad/s$. Formulas and values to compute the motor input conditions are the same of the precedent paragraph. Final values are listed in the above table:

	DATA	
θ_{eq}	45°	Pendulum required angle
ω	$10^{rad}/s$	Sphere desired velocity
	RESULTS	
I	$4.94A$	Motor required current
V	$24.40V$	Motor required voltage

Table 3.3: Data and results of main pendulum motors for slope climbing. The obtained current allows a continuous operative control of the rover since maximum continuous current injected by Maxon drivers is 5A [5].

3.5   Working condition for step climbing

The condition for the step climbing is achieved starting from a standstill situation with the pendulum in static position.

First, the pendulum reaches an angle of 90°.

Then, torque is generated through the CMGs to overcome the obstacle. The implementation of gyroscopic torque is necessary in situations where it is not possible to position the system's COM aligned with the step edge. Therefore, an important design objective is to have the barycenter as low as possible.

Lowering the system's center of mass allows to overcome higher obstacles through pendulum motors' actuation only. This makes the system more power-efficient since the CMGs consume a considerable amount of battery charge to overcome just one step.

CMG torque formula has already been explained in chapter "Design review" in paragraph "Spinning motors of CMG" of part 1. Knowing the system geometry and masses it is possible to determine the maximum required τ_G starting from equation 3.1:

$$\tau_{G_{MAX}} = \left(\sqrt{2Rh - h^2} - a \right) M_{TOT}\, g \tag{3.9}$$

In [2], it was computed that maximum needed torque is $25.82 Nm$. After the design review, the obtained values listed in table 8.1 lead to a maximum torque of $25.42 Nm$. As expected, a rover with a lower center of mass requires a lower generated torque. Since the required torque is lower, the values of spinning and tilting speed need to be reduced. It was decided to decrease the spinning speed because the tilting speed determines the maneuver time execution. If time of the execution increases the consumption deriving from pendulum motors and spinning motors increases.

Step climbing analysis was conducted by studying every motor working conditions. The first condition to be examined is to hold the pendulum at 90° with respect to the resting axis. Applying the moment formula previously discussed in section 3.3, the torque to be applied is $20.84 Nm$.

When CMGs are activated, the torque required by the motors increases to maintain the pendulum static. The total torque at the differential box output rises up to

$46.26Nm$. Using the precedent formulas, the following values are obtained:

	no CMG	**CMG**
τ_P	$20.84Nm$	$46.26Nm$
I	$6.98A$	$15.50A$

Table 3.4: Pendulum torque and relative motor current depending on CMG action.

The maximum computed current exceeds the peak current of the motor. However, the maximum torque is required for a fraction of a second, thus no damages are expected.

CMG motor velocities are now analysed.

$$\vec{\tau_G} = I_{fl}\,\vec{\omega} \wedge \vec{\Omega} \tag{3.10}$$

Starting from 3.10 (derived in Part 1), it is obtained that the new spinning speed must be $7890rpm$. Introducing a safety factor of 0.95, the required speed becomes $8305rpm$. Needed torque, computed in [2], is $52mNm$.
The Maxon website allows the customer to compute voltage and current requested by motors
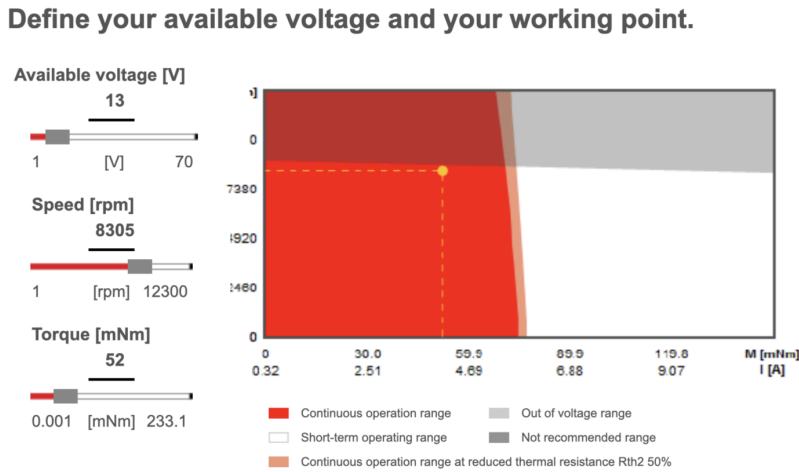
Figure 3.3: Maxon tool for DCX 35 L motors.

Final derived values are $V = 12.42V$ and $I = 4.12A$. As can be seen in Figure 3.3, motors operating point is inside continuous operating range.

Tilting motors are always excited to maintain in standstill position the CMG groups. The required torque slightly decreases during the execution of the manoeuvre. The required current is considered constant and equal to the maximum value of $400mA$.

3.6 Power consumption analysis

All consumption information for the different situations is known.
To determine the required consumption, the operational time for each working state must be defined. As previously discussed, the objective of the sizing process is to include the different working situations. In this way, the final consumption obtained from the sizing process is representative of a realistic environment, characterized by different conditions.

Conservative assumptions have been set to determine the needed values with safe margins. The goal is to achieve 1 hour of operation, before charging again the batteries. The rover must be able to work at nominal speed and must be able to climb a minimum number of steps.

The final choice for consumption computation was to perform a trade-off between plain and slope situations. The selected trade-off is 75%, i.e. the goal is to advance for at least 45 minutes on flat surfaces and 15 minutes on inclined ones.
For CMG consumption, a minimum of 5 steps to overcome was established.
It is possible to determine the necessary electric charge for operation over a given period by integrating the current demand curve over the selected time interval. Since constant current consumption is assumed, computations are performed by simply multiplying time and current .

3.6.1 CMG consumption

The consumption of the gyroscopic maneuver depends on the time required by the spinning motors to reach the desired speed, the time necessary to raise the pendulum by 90°, and the rotation time of the CMGs. The initial condition of the maneuver assumes the rover is stationary and in contact with the step to be overcome.

From previous studies conducted on the spinning motors, it has been estimated that the steady-state speed can be reached in 16 seconds [2]. This duration has been used as a reference for the consumption calculations. With dedicated control, the transient can be significantly reduced.

At this point in the discussion, it has not yet been possible to define the lifting speed of the pendulum. Since the actuation is performed by the pendulum motors, it is expected the developed control system to be able to achieve this condition with a reduced transient. For the analysis, it has been assumed that elevation and stabilization lasts 3 seconds. The pendulum is raised only after the spinning motors have reached steady-state speed.

Finally, the effective duration of the maneuver depends on the tilting motors. The expected speed is $15rpm$, which means that to perform the entire 90° rotation 1 second is required.
In total, the expected duration of the maneuver is 20 seconds.

Spinning motors are the first motors to start up and require constant torque throughout their operation. This implies that the current remains constant throughout the entire manoeuvre. The capacity required for a single motor is:

$$20s \cdot 4120A = 22.89mAh$$

The stepper motors are constantly energised, the expected current consumption is 0.4A continuously. Considering the manoeuvre duration time of $20s$, motor consumption results as:

$$20s \cdot 0.4A = 2.22mAh$$

The motors that account for the highest consumption are those of the pendulum. Their operation is divided into two parts, the pendulum's elevation phase and the holding phase.
In the first phase, the torque required of the pendulum varies from $0Nm$ to $20.84Nm$. In the previous section, it was seen that the current consumption for the final elevation of the pendulum is $6.98A$. The variation in current demand has a form corresponding

to the first quarter period of a sinusoid. By integrating the trend for time, the corresponding charge can be obtained. It was decided to consider the maximum and constant current demand throughout the time period as a conservative assumption. The result is:

$$3s \cdot 6.98A = 5.82mAh$$

Once in position, the torque goes from $20.84Nm$ to $46.26Nm$. As before, assumption of a constant maximum current is made. The consumption is:

$$1s \cdot 15.5A = 4.3mAh$$

The table below shows the calculated values and total manoeuvre consumption for a single CMG unit and a single pendulum motor.

Motor	Time	Current	Charge
Spinning	$20s$	$4.12A$	$22.89mAh$
Tilting	$20s$	$0.40A$	$2.22mAh$
Pendulum (no CMG)	$3s$	$6.98A$	$5.82mAh$
Pendulum (CMG)	$1s$	$15.5A$	$4.30mAh$
TOTAL			$35.23mAh$

Table 3.5: Consumption of a single group of motor to active CMG maneuver

3.6.2   Total consumption

It is now possible to compute the total required capacity C of the system as:

$$C = 2 \cdot (I_{plane} \cdot 0.75\,t + I_{slope} \cdot 0.25\,t + I_{tilting} \cdot t + I_{CMG} \cdot N) \qquad (3.11)$$

where t is the total operative time and N is the number of the desired steps.

The following table reports the computed currents for the single motors. At the end is reported the required capacity from the whole system for $1h$ of operativity and for $N = 5$ steps to climb.

Motor	Current	Capacity
Pendulum (plain)	A	-
Pendulum (slope)	$4.94A$	-
Tilting	$0.40A$	-
CMG system (N=1)	-	$35.23mAh$
Capacity ($1h$)		$3.34Ah$

Table 3.6: Current required by single motors.

Electronics consumption were not taken into account since a separated power supply was chosen. It was esteemed the electronics charge consumption to be under $1Ah$. Power supply consists of two $9V$ rechargeable Li-ion batteries. This guarantees sensors independence from the rest of the system.

3.7 Battery choice

The battery to be selected must be able to cover the computed capacity. It must also be greater than required voltage, i.e. the $24.89V$ of the pendulum motors measured in Table 3.3.

After some research, the chosen batteries are a pair **MaxAmps Li-ion 5000 8S1P 28.8v Battery Pack**. Their weight of $576g$ was already predicted in the table 3.1. They have a voltage of $28.8V$ and a capacity of $5Ah$. Assuming an efficiency of 0.85, the useful capacity is $4.25Ah$. By connecting the batteries in parallel, the total power supply of the system has $28.8V$ voltage and a theoretical capacity of $10Ah$.

For the application considered in Section 3.6.2, the rover can be constantly powered for 78 minutes before the next charge. Or also, it can last 60 minute respecting the imposed trade-off but with the possibility to climb $N = 17$ steps.

Finally, basing on the initial goal to work constantly in nominal conditions, the batteries would last about 48 minutes.
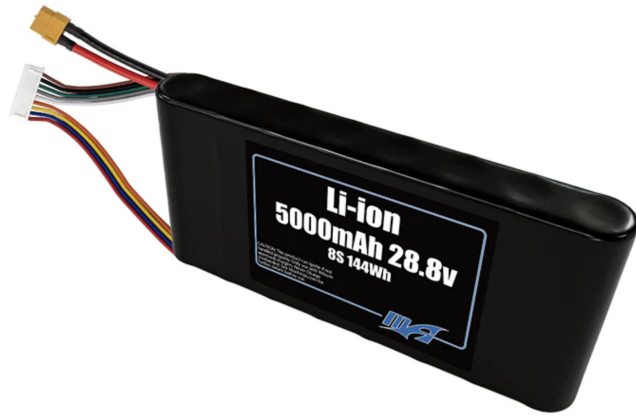
Figure 3.4: MaxAmps battery.

Chapter 4

Multibody plant system in Simulink/Simscape and analytical dynamical model

4.1 Introduction

In this Chapter is discussed the generation of a multibody plant system and the derivation of the dynamical equation of the model. The starting point of the multibody model developement is the SolidWorks CAD assembly representing the final rover design. An equivalent block diagram construction has been made in Simulink/Simscape environment. Finally, a complete and high fidelity representation of the physical model was obtained by modelling blocks interactions and dynamics. Three main different version of the multibody have been derived starting from the first one. For analytical model development, a dynamics study has been conducted based on the Euler-Lagrange formulation.Non-slip constraint condition were imposed to solve the lagrangian multiplier problem and to obtain the final equations. In order to validate all the derived model, different sets of simulation were performed.

4.2   Multibody Plant

The multibody representation of a plant consist of representing the studied physical object through the connection of different bodies. The connection could be rigid or made by a specific joint typology. For generating the plant system it was used the Solidworks tool "Simscape multibody link" that permits to generate an ".xml" file that stores all the couplings and all the inertia data of the different parts. The exported files were used in MATLAB/Simulink and in particular into Simscape multibody environment. Once generated this file and imported in Simulink, the next step was to correct it and represent properly every mechanism.

To faithfully reproduce every relative movement between the components, its important to analyse in detail the motion transmission. Motion is generated from the motors in the bottom part of the pendulum. Motors are welded respect to pendulum structure by using specific plates. Motion is transmitted to the lateral shafts of differential gox by implementing pulleys and belts . The connection of these components was designed such that a positive rotation of the Motor Pulley 1 corresponds to a positive rotation of the Lateral Shaft 1, while positive rotation of the Motor Pulley 2 correspond to a negative rotation of the Lateral Shaft 2 as shown in fig 4.1.
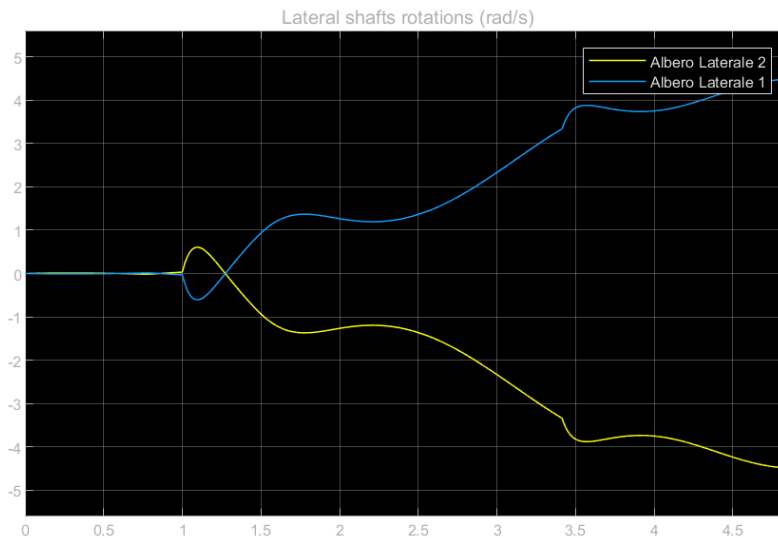
Figure 4.1: Speed behaviour of Lateral Shaft 1 (blue line) and Lateral Shaft 2 (yellow line)

To represent the differential mechanism, bevel gear constraint with the designed bevel

gear dimensions is presented. It is important to set the reference systems of all three gears reporting the Z-axis that coincides at the same point.

To represent the differential mechanism, bevel gear (fig. 4.2) connections were performed. The implemented Bevel Gear blocks are joint to the lateral shafts. Their interaction transmits the motion to the main shaft. The connection between a shaft and its bevel gear is performed by imposing z-axis coincidence.
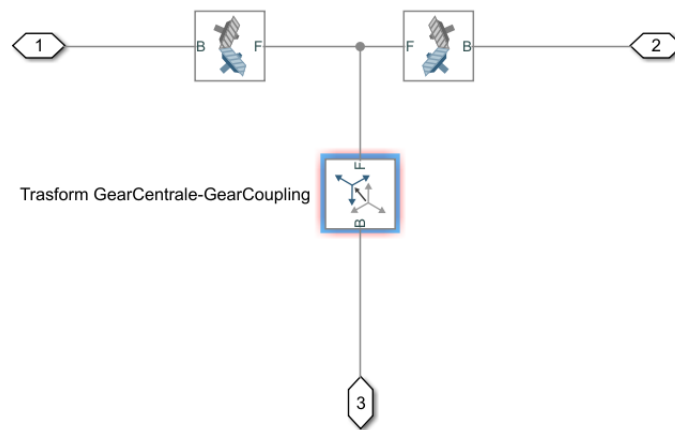
Figure 4.2: Bevel constraint

For the sphere-plane system, the spatial contact force block (fig. 4.3) is used with the following damping and stiffness parameters to simulate a realistic contact between the plexiglass spherical shell and the ground. Stiffness= $1e10^{-6}N/m$; Damping=$1e10^{-3}N\,s/m$. Values both static and dynamical friction coefficients, the value was assumed to be unitary. This implies the maximum friction is acting between shell and plane.
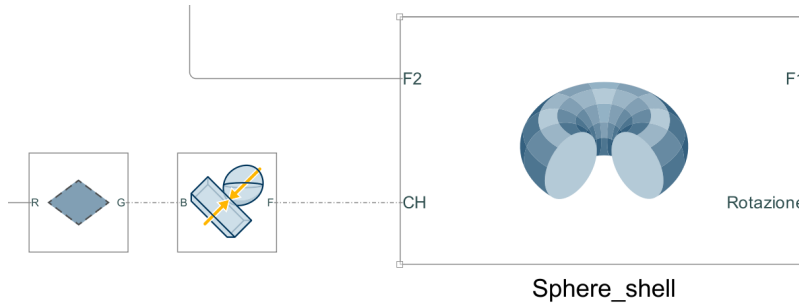
Figure 4.3: Spatial contact force

Another type of contact between the two bodies was modeled using the Point Contact Cloud, fig. 4.4, creating an arbitrary number of contact spheres along the rover's spherical surface.
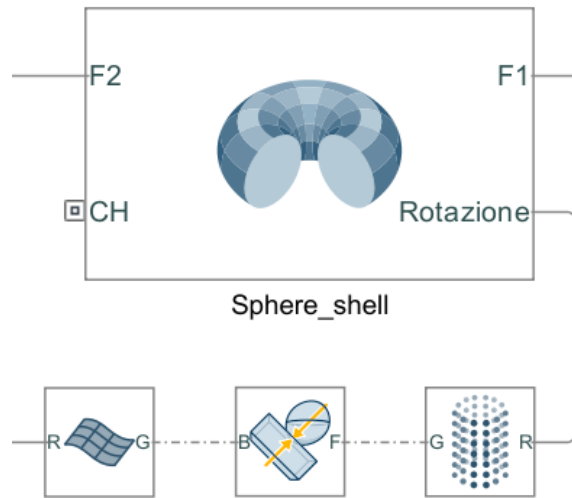
Figure 4.4: Point cloud

This method successfully simulated the robot within a custom terrain. However, this approach requires significant computational capacity, making real-time control of the rover impossible to actuate. A denser point cloud creates a more realistic model but drastically increases the number of calculations.

The final representation in MATLAB/Simulink Mechanics explorer is represented in figure 4.5
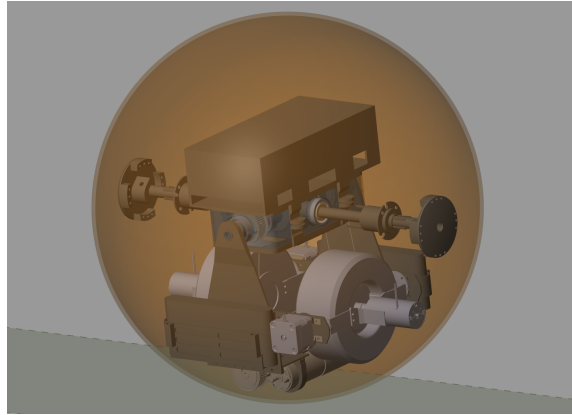
Figure 4.5: Simscape model

4.3   Semplified Configurations

After accurately modelling the spherical rover, a second Simscape model was built to reduce computational load and execution time in MATLAB without compromising performance, accuracy, and reliability. The first model needs around 720.828 seconds in order to simulate 1 second. Additionally, a third file representing the rover in extremely simplified form was developed, in order to minimize the number of components and relative motions to only the most essential joints.

As is going to be shown from the simulations, the two simplified models prove to be suitable for controller development. In particular the second one show a good level of similarity to the initial plant system.

4.3.1   Development of second plant version

Differences between the second model respect to the first one are listed:

- The CMG devices are be fixed to the pendulum and incapable of movement, in order to simulate the rover's performance without the actuation of the gyroscpic maneuver.

- Welded joints are eliminated since it was noticed they do not provide higher simulation performances.

- Rigid transformations are significantly reduced and condensed to a minimum number.

- Scopes and reference systems generated on the bodies are removed.

The final result of the plant is shown in Figure 4.6:
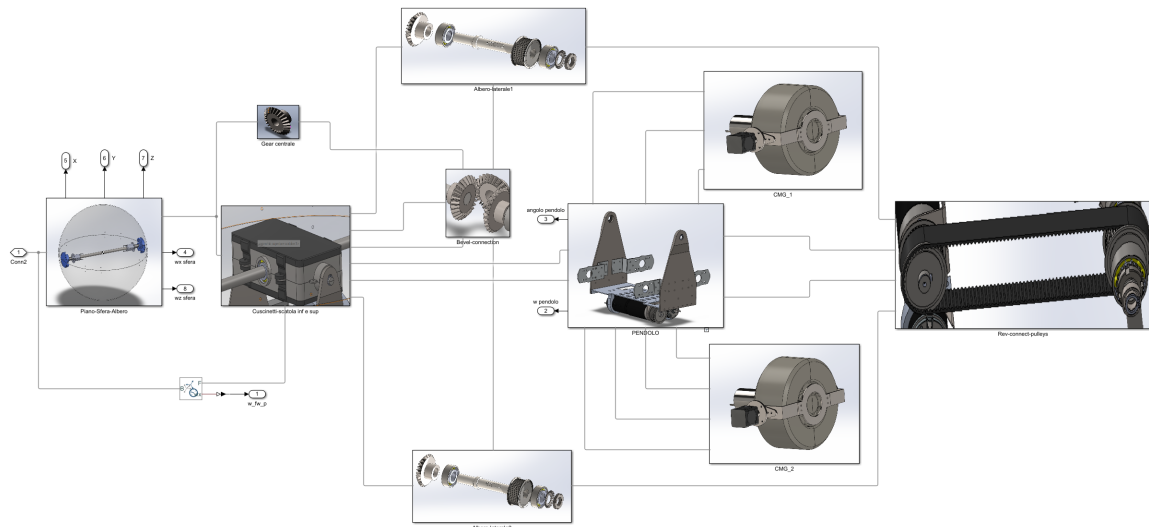
Figure 4.6: Second plant version

4.3.2 Development of a third plant version

After developing the second version of the plant, the simulation runtime was approximately 10.386 seconds for 1 simulation second choosing an ODE45 solver. However choosing a DAE solver, time computation drastically decrease and so test results are quickly shown. Insted results challenging to control the robot real-time with a simulation pacing of 1 second. Therefore, to enable real-time control, a third more simplified version of the plant was developed.

This version presents a drastic reduction in the number of single mass bodies. In fact, the number of masses in the file is condensed five assemblies, corresponding to:

- Main shaft, central bevel gear, counterweight, and cross joint assembly

- Pendulum group, motor, and CMG assembly

- Differential box shell and cases assembly

- Lateral shafts 1 and 2 and relative transmission components assemblies

- Case with electronic components Each assembly was redesigned in SolidWorks and imported to Simulink, with new defined values of mass, center of gravity, and moments of inertia. The final model is shown in Figure 4.7:
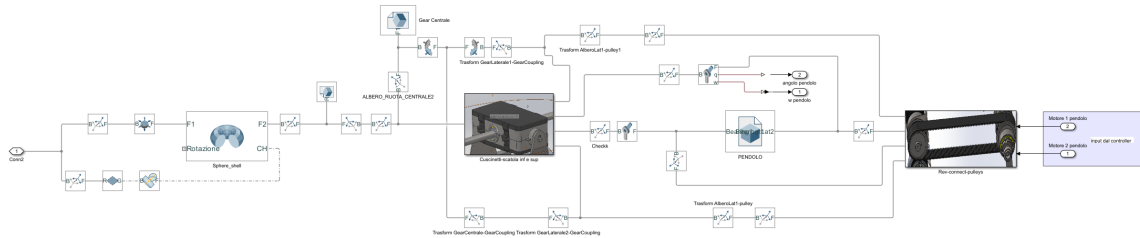
Figure 4.7: Third plant version

The model demonstrates high execution efficiency, as it takes 682.25 milliseconds to generate 1 second of simulation. The selected Simscape solver is the DAE. The obtained model permits real time simulation with good smoothness

4.4 Open loop simulation and validation

In order to simulate the Rover behavior, it has been taken in consideration the virtual analytical model of the motors. In addition it has been set the surface typology and input reference.

4.4.1 Motor representation

The brushed DC motor RE 40, responsible for motion actuation, is represented as described in [2] using a classical schematic. An internal control system based on the input current is added, to ensure the motor follows the input reference. Consequently, the revolute joint between the motor and the pulley is actuated in torque and motor speed is implemented as feedback term, as shown in Figures 4.8 and 4.9
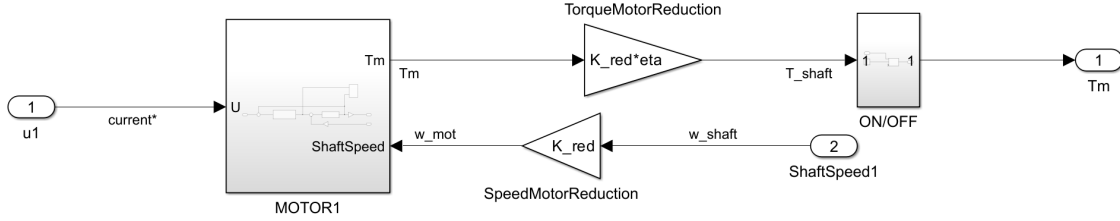
Figure 4.8: Current reference to torque [2]
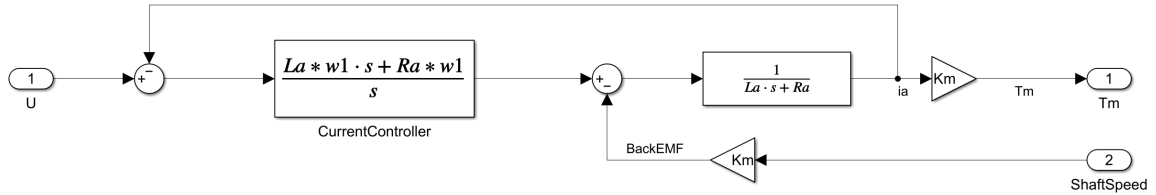
Figure 4.9: Motor with iternal controller ([2]

4.4.2   Surfaces and Reference signals

For input generation, three different options were used: Step signal, Signal Builder, and joystick controller.

The virtual surface is generated depending on the conducted simulation. The presented surface are: simple plane and custom surface.

The flat surface was simulated using simple infinite surface block, as show in Figure 4.3. This type of surface can be implemented also in inclined plane generation. By modify the gravity vector, distribution of its components along the y-axis (vertical axis) and z-axis (longitudinal axis) can be performed according to the formula:

$$[0,\, g\cos(\alpha),\, g\sin(\alpha)]\,. \tag{4.1}$$

Another method involves the implementation of a rigid transformation between the world frame and the plane frame. This transformation consists of a rigid rotation along the lateral axis (in this case, the x-axis) by the plane's desired inclination

angle. A positive inclination corresponds to the robot going downhill, a negative one corresponds to an uphill surface.
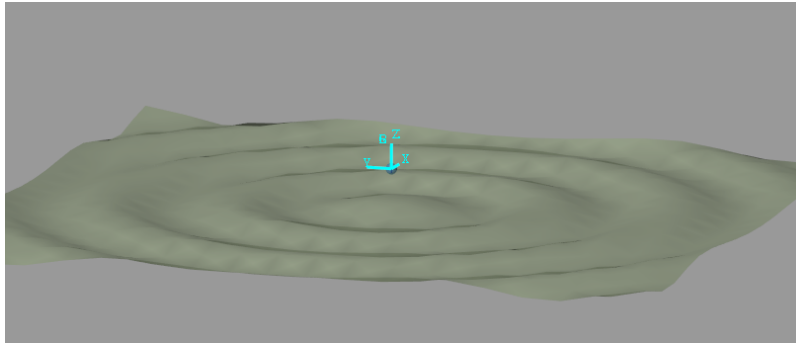
Figure 4.10: Custom surface

To represent a custom surface, the Grid Surface block is implemented as shown in Figure 4.4. Matrices can be constructed to represent the desired surface. To set a sinusoidal surface, as shown in Figure4.10, the script code below was executed to generate the needed matrices to inserted in the blocks

The following MATLAB code generates a 20x20 (m) grid surface using a sinusoidal function:

```matlab
% Grid surface
GRID_1 = linspace(-10, 10, 20);

% Dimensions of the matrix
rows = 20;
cols = 20;

% Initialize the matrix
sinMatrix = zeros(rows, cols);

% Create a vector of x values to evaluate the sine
x = linspace(0, 6*pi, cols);

% Populate the matrix using a for loop
for i = 1:rows
    sinMatrix(i, :) = sin(x);
end

% Dimensions of the matrix
n = 20;

% Create a range of values for x and y
x = linspace(-6*pi, 6*pi, n);
y = linspace(-6*pi, 6*pi, n);

% Create a 2D grid
[X, Y] = meshgrid(x, y);

% Calculate the 3D sine function
GRID_2 = sin(sqrt(X.^2 + Y.^2)) * 0.2;
```

Inputs

The chosen reference value are mainly two. The first one consist of the reference linear velocity (m/s), while the second is an angle reference (deg), more specifically the angle defined between the pendulum and the main shaft in a lateral configuration.

This inputs are generated on MATLAB/Simulink by three block typology, as they are showed in fig.4.11. The first is a step input. The second is a signal generator, that allows to design linear signal profiles. The last one is a joypad input. Thanks to this block a physical joystick via serial port can be connected to Simulink and generate various signal that could be boolean - 0 & 1 - or Integers in a specific range (for instance, joystick signal vary between -127 and 127).
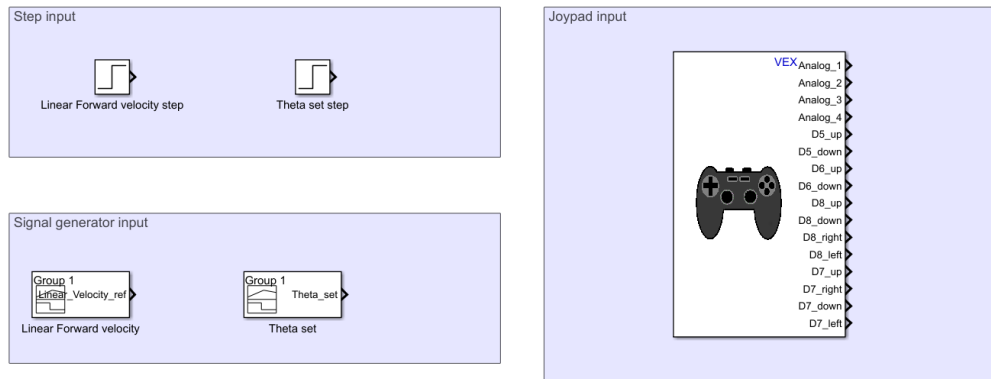
Figure 4.11: Inputs

4.4.3   Results

The first multibody model generated, is considered as "high fidelity" since it faithfully reproduces each component and relative motion among them. For this reason, the simplified plant model versions are compared with this one.

Stepping up to the comparative simulations between the first two models, open-loop tests were performed.

The selected input to perform the following tests is step input block and it is directly connected to the revolution joint representing the motor. The reference input is measured in torque (Nm).

Two test typologies have been considered:

- The former, performing a longitudinal motion maneuver. The input to the two motors are of equal in boyh modulus $(0.5Nm)$ and sign.

- The second one is performed feeding to motors, 2 torques of equal modulus but opposite direction, in order to generate curved trajectory.

The results of the described tests are displayed below. Especially the figure 4.12 shows the robot trajectory along "X", "Y" and "Z" coordinates while performing the straight path motion. Figure 4.13, on the other hand, shows the values of:

- Motor 1 Torque as input step (Nm)

- Motor 2 Torque as second step input (Nm)

- The relate motors angular velocity (rad/s)

- The lateral θ angle formed by the pendulum and the main shaft (rad)

- The forward and lateral angular velocity of the pendulum (rad/s)

- The forward and lateral sphere angular velocity (rad/s)
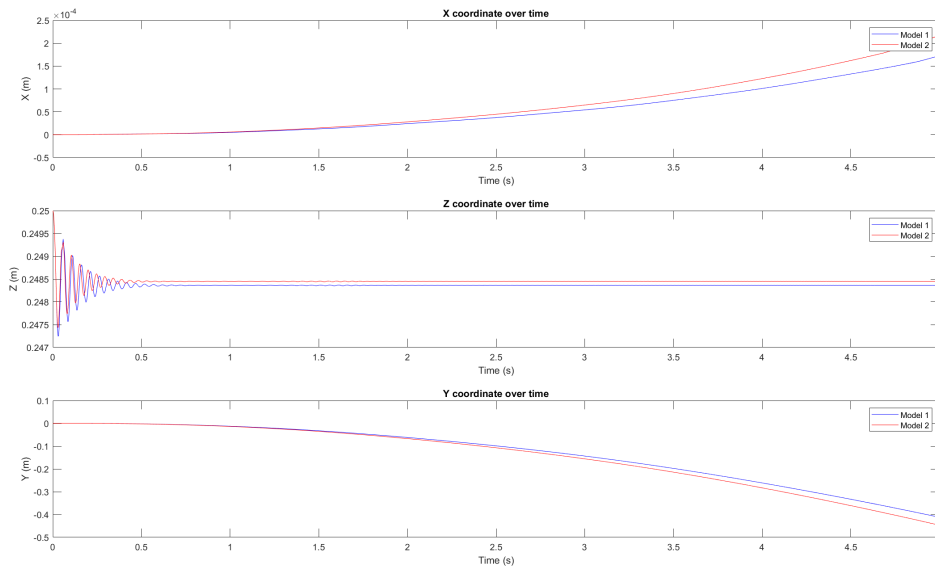
Figure 4.12: Model 1 and 2 trajectory
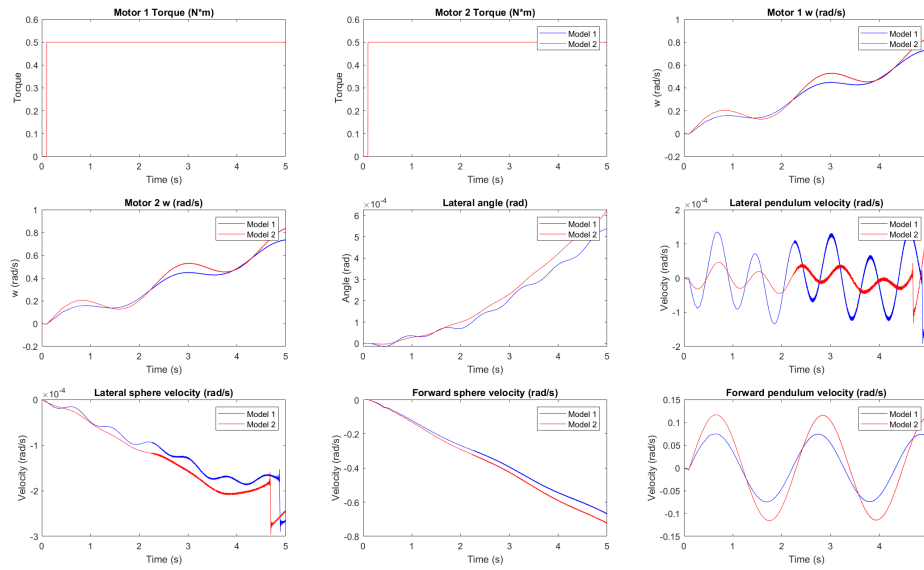
Figure 4.13: Model 1 and 2 performance test n°1

Same approach was followed for the second simulation. Test 2 performances are presented:
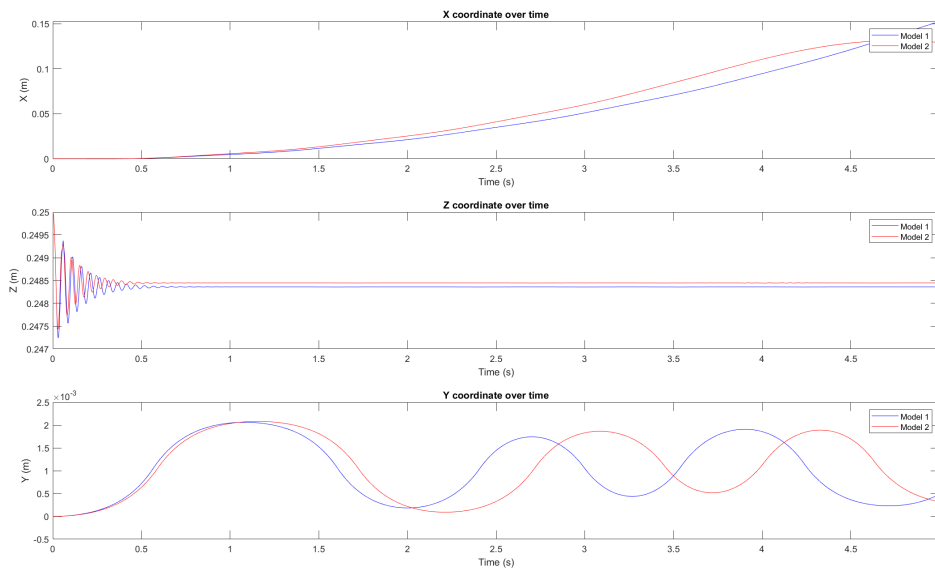
Figure 4.14: Model 1 and 2 trajectory
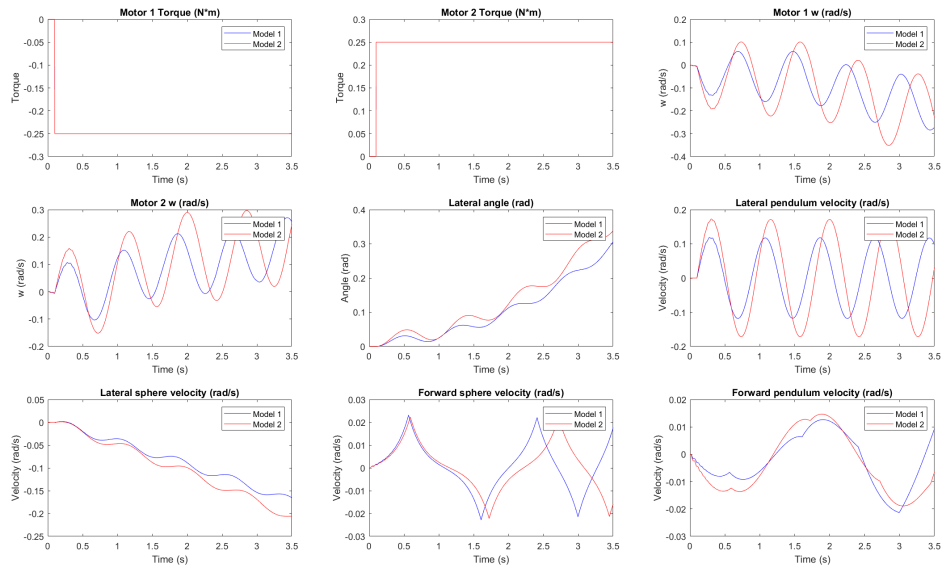
Figure 4.15: Model 1 and 2 performance test n°2

As can be seen from the MATLAB plots, the data generated from the second multibody follow with high accuracy the performance of the first model.

For this reason it has been confirmed the reliability of the second model and the capability of transpose the results made for this model as the true one of the Rover. As previously stated were made tests for the comparison between all the three model. Hence with the identical approach, the performance simulation are presented in the following figure:
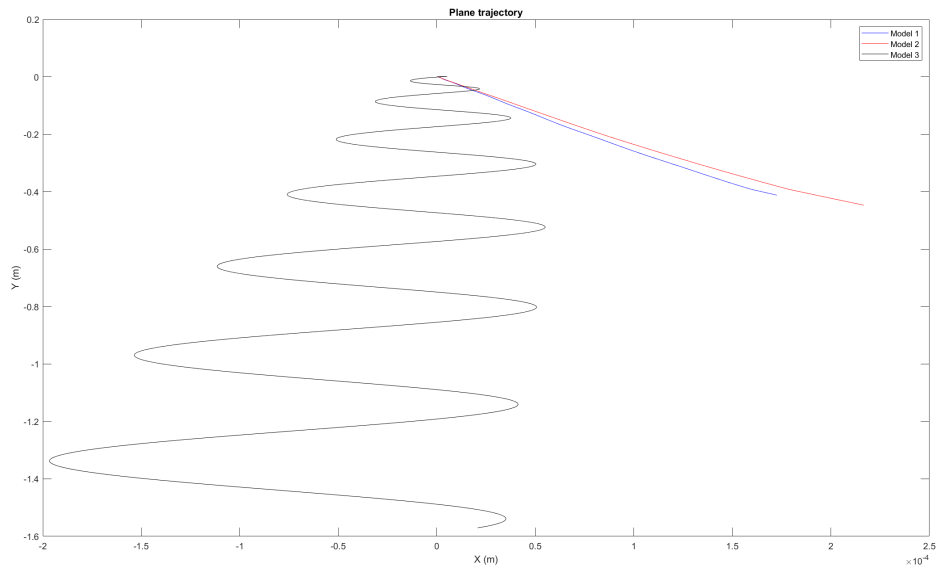
Figure 4.16: Planar trajectory of all 3 models
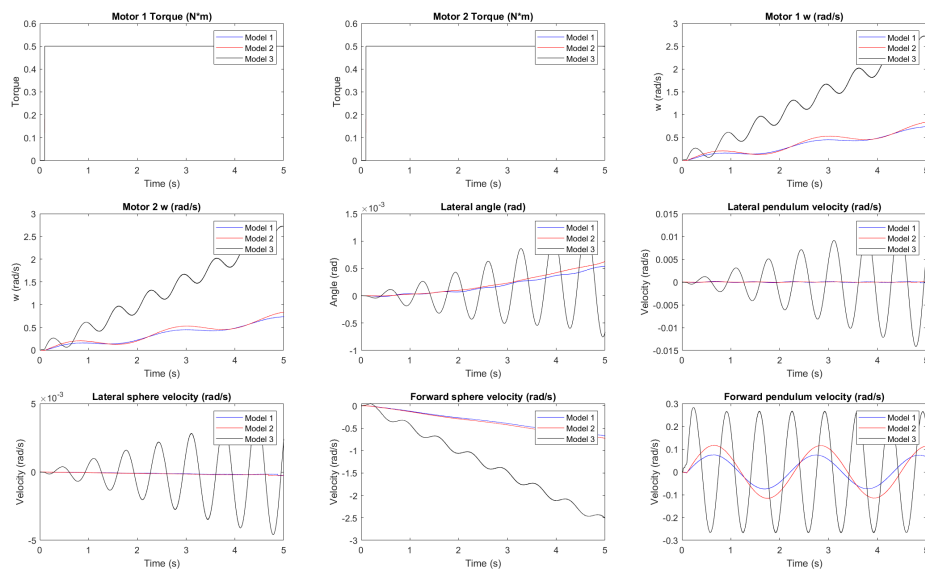
Figure 4.17: Performance test among all 3 models
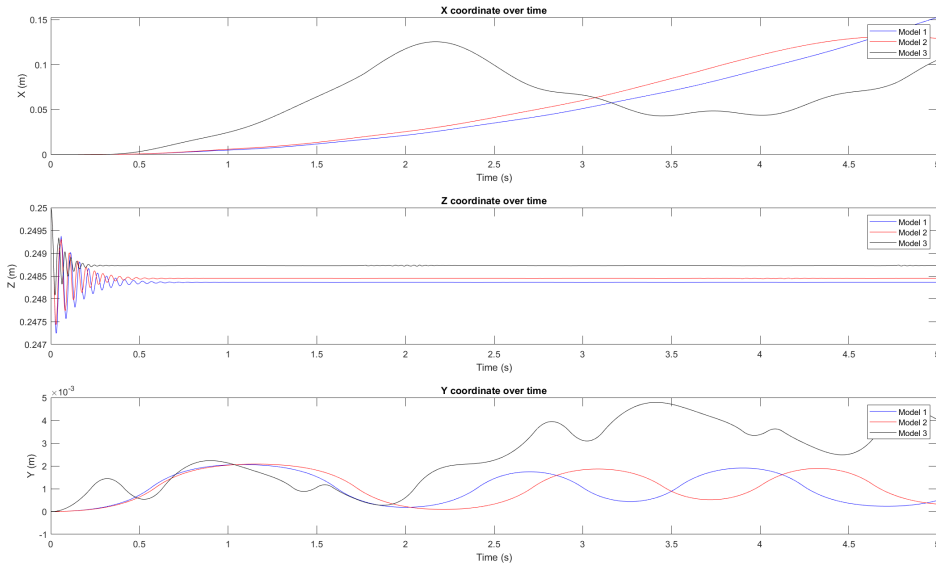
Figure 4.18: Position over time of all 3 models
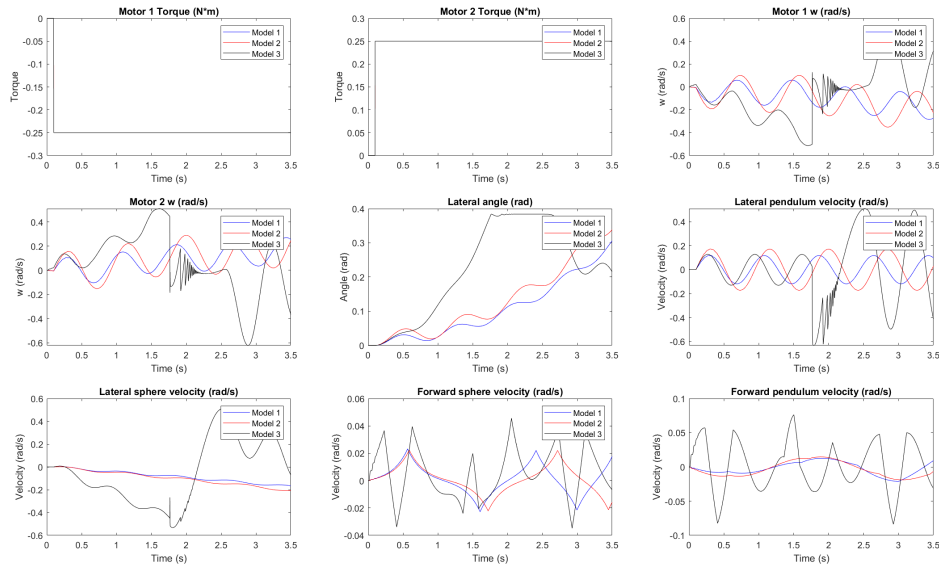
Figure 4.19: Performance test among the 3 models

In figure 4.16, 4.17 it has been represented the simulation made for the straight trajectory motion. Thus, the figures 4.18 and 4.19 describe all the three models

behaviour during a lateral side path trajectory. In the third model, the parameter trend shows too much deviation compared to the first two models behaviour. For this reason, the third model has been declared as too simple and inconsistent, although a reliable multibody plant definition. The controller design problem, addressed in the next chapter, has been implemented only in the second version of the multibody plant.

4.5 Analytical Model

4.5.1 Problem definition

In this section, we address the analytical model definition problem, ending with the equations of dynamics computation.

The robot is represented as consisting of four main masses: the sphere, the differential, the electronics and the pendulum.

For proper modeling the analytical system, it is essential to accurately define the reference frames related to each of these masses starting from the Frame world.

The derivation of the dynamic model begins from the evaluation of the kinematics model of the system. The positions and velocities of the masses are defined using the reference systems just introduced. The generalized coordinates describe the configuration of the robot in terms of angular and linear positions. A crucial aspect of the problem is the non-holonomic constraint imposed by the contact between the sphere and the plane, which must satisfy the pure rolling condition:

$$\boldsymbol{v}_{\text{sfera}} = \boldsymbol{\omega} \times \boldsymbol{r} \tag{4.2}$$

The dynamics robot's equations are then derived by considering the kinetic energy, potential energy, external forces and system constraints. This yields to a complete set of equations describing the dynamic behavior of the spherical robot in response to inputs.

4.5.2 Kinematics

Matrices for rotation and translation from world frame to sphere frame are described. The Sphere Frame can be represented by 3 sequential rotation respect to World frame. These 3 rotation are indicated by the RPY angles

$$[\theta_x, \theta_y, \theta_z]$$

$$R_{w\_s1} = \begin{bmatrix} \cos(\theta_z) & -\sin(\theta_z) & 0 \\ \sin(\theta_z) & \cos(\theta_z) & 0 \\ 0 & 0 & 1 \end{bmatrix} \tag{4.3}$$

$$R_{s1\_s2} = \begin{bmatrix} \cos(\theta_y) & 0 & \sin(\theta_y) \\ 0 & 1 & 0 \\ -\sin(\theta_y) & 0 & \cos(\theta_y) \end{bmatrix} \tag{4.4}$$

$$R_{s2\_s} = \begin{bmatrix} 1 & 0 & 0 \\ 0 & \cos(\theta_x) & -\sin(\theta_x) \\ 0 & \sin(\theta_x) & \cos(\theta_x) \end{bmatrix} \tag{4.5}$$

The final rotation matrix is computed as below:

$$R_{w\_s} = R_{w\_s1} R_{s1\_s2} R_{s2\_s} \tag{4.6}$$

$$t_{w\_s} = \begin{bmatrix} x \\ y \\ R \end{bmatrix} \tag{4.7}$$

$$T_{w\_s} = \begin{bmatrix} R_{w\_s} & t_{ws\_w} \\ 0 & 1 \end{bmatrix} \tag{4.8}$$

Matrix T_{w_s} is the homogeneous matrix and includes translation vector inside.
After obtaining the sphere frame homogeneous matrix, now to describe the differential frame we begin from sphere one, in fact the differential mass move identically as the sphere apart of a subsequent rotation about the y-axis of α angle :

$$R_{s\_d} = \begin{bmatrix} \cos(\alpha) & 0 & \sin(\alpha) \\ 0 & 1 & 0 \\ -\sin(\alpha) & 0 & \cos(\alpha) \end{bmatrix} \tag{4.9}$$

$$t_{s\_d} = \begin{bmatrix} 0 \\ 0 \\ 0 \end{bmatrix} \tag{4.10}$$

44

$$T_{s\_d} = \begin{bmatrix} R_{s\_d} & t_{s\_d} \\ 0 & 1 \end{bmatrix} \tag{4.11}$$

The electronics group kinematics is derived starting from the differential one, as they rotates perfectly equal, but the Electronic mass is located above the differential mass and so present an offset quantity of $(+le)$:

$$R_{d\_e} = \begin{bmatrix} 1 & 0 & 0 \\ 0 & 1 & 0 \\ 0 & 0 & 1 \end{bmatrix} \tag{4.12}$$

$$t_{d\_e} = \begin{bmatrix} 0 \\ 0 \\ +le \end{bmatrix} \tag{4.13}$$

$$T_{d\_e} = \begin{bmatrix} R_{d\_e} & t_{d\_e} \\ 0 & 1 \end{bmatrix} \tag{4.14}$$

Finally the last considered mass consist of the pendulum element. In order to derive the kinematics related to the attached frame, it must be considered that pendulum group, is able to further rotate about the x-axis of a β angle quantity and the COM of it is shifted from differential frame by a $-lp$ offset.
Then the Homogeneous matrix is computed as follows:

$$R_{d\_p1} = \begin{bmatrix} 1 & 0 & 0 \\ 0 & \cos(\beta) & -\sin(\beta) \\ 0 & \sin(\beta) & \cos(\beta) \end{bmatrix} \tag{4.15}$$

Frame $p1$ is an intermediate frame between differential and pendulum, ensuring rotation of β along x_d and translation of $-lp$ along z_{p1}:

$$R_{p1\_p} = \begin{bmatrix} 1 & 0 & 0 \\ 0 & 1 & 0 \\ 0 & 0 & 1 \end{bmatrix} \tag{4.16}$$

$$t_{d\_p1} = \begin{bmatrix} 0 \\ 0 \\ 0 \end{bmatrix} \tag{4.17}$$

$$t_{p1\_p} = \begin{bmatrix} 0 \\ 0 \\ -lp \end{bmatrix} \tag{4.18}$$

Vectors representing positions referred to the world frame:

$$\text{Center of sphere: } \mathbf{p}_s = \begin{bmatrix} x \\ y \\ R \end{bmatrix} \tag{4.19}$$

$$\text{Center of mass of differential: } \mathbf{p}_d = \begin{bmatrix} x \\ y \\ R \end{bmatrix} \tag{4.20}$$

Electronics group COM computation:

$$R_{w\_d} = R_{w\_s} R_{s\_d} \tag{4.21}$$

$$T_{w\_d} = \begin{bmatrix} R_{w\_d} & \mathbf{p}_d \\ 0 & 1 \end{bmatrix} \tag{4.22}$$

$$\mathbf{t}_{w\_e} = T_{w\_d} \begin{bmatrix} \mathbf{t}_{d\_e} \\ 1 \end{bmatrix} \tag{4.23}$$

$$\mathbf{p}_e = \begin{bmatrix} \mathbf{t}_{w\_e}(1) \\ \mathbf{t}_{w\_e}(2) \\ \mathbf{t}_{w\_e}(3) \end{bmatrix} \tag{4.24}$$

pendulum COM computation:

$$\mathbf{p}_{p1} = \begin{bmatrix} x \\ y \\ R \end{bmatrix} \tag{4.25}$$

$$R_{w\_p1} = R_{w\_s} R_{s\_d} R_{d\_p1} \tag{4.26}$$

$$T_{w\_p1} = \begin{bmatrix} R_{w\_p1} & \mathbf{p}_{p1} \\ 0 & 1 \end{bmatrix} \tag{4.27}$$

$$\mathbf{t}_{w\_p} = T_{w\_p1} \begin{bmatrix} \mathbf{t}_{p1\_p} \\ 1 \end{bmatrix} \tag{4.28}$$

$$\mathbf{p}_p = \begin{bmatrix} \mathbf{t}_{w\_p}(1) \\ \mathbf{t}_{w\_p}(2) \\ \mathbf{t}_{w\_p}(3) \end{bmatrix} \tag{4.29}$$

Velocity vectors referred to the world frame:

$$\text{Center of sphere: } \mathbf{v}_s = \begin{bmatrix} dx \\ dy \\ 0 \end{bmatrix} \tag{4.30}$$

$$\text{Center of mass of differential: } \mathbf{v}_d = \begin{bmatrix} dx \\ dy \\ 0 \end{bmatrix} \tag{4.31}$$

$$\text{Velocity of electronics box: } \mathbf{v}_e = \frac{d\mathbf{p}_e}{dt} \tag{4.32}$$

(Explicit equation in Appendix 8.1)

$$\text{Velocity of pendulum: } \mathbf{v}_p = \frac{d\mathbf{p}_p}{dt} \tag{4.33}$$

(Explicit equation in Appendix 8.2)

The Sphere angular velocity can be obtained by the Skew-symmetric matrix compu-

tation $\boldsymbol{S}_s$ defined by the derivative of the Rotation matrix $\boldsymbol{R}_{w_s}$ multiplied by his own transpose.

The generated equation are presented as follows:

$$\boldsymbol{S}_s = \frac{d\boldsymbol{R}_{w\_s}}{dt}\boldsymbol{R}_{w\_s}^{\top} \tag{4.34}$$

The angular velocity vector $\boldsymbol{w}_s$ is then obtained from the entries of the matrix $\boldsymbol{S}_s$ in the indicated position:

$$\boldsymbol{w}_s = \begin{bmatrix} \boldsymbol{S}_s(3,2) \\ \boldsymbol{S}_s(1,3) \\ \boldsymbol{S}_s(2,1) \end{bmatrix} \tag{4.35}$$

(Explicit equation in Appendix 8.3)

Velocity of differential and electronics system

$$\boldsymbol{S}_d = \frac{d\boldsymbol{R}_{w\_d}}{dt}\boldsymbol{R}_{w\_d}^{\top} \tag{4.36}$$

$$\boldsymbol{S}_e = \boldsymbol{S}_d \tag{4.37}$$

$$\boldsymbol{w}_d = \begin{bmatrix} S_d(3,2) \\ S_d(1,3) \\ S_d(2,1) \end{bmatrix} \quad \boldsymbol{w}_e = \begin{bmatrix} S_e(3,2) \\ S_e(1,3) \\ S_e(2,1) \end{bmatrix} \tag{4.38}$$

(Explicit equation in Appendix 8.4)

Velocity of pendulum system

$$\boldsymbol{S}_p = \frac{d\boldsymbol{R}_{w\_p}}{dt}\boldsymbol{R}_{w\_p1}^{\top} \tag{4.39}$$

$$\boldsymbol{w}_p = \begin{bmatrix} S_p(3,2) \\ S_p(1,3) \\ S_p(2,1) \end{bmatrix} \tag{4.40}$$

(Explicit equation in Appendix 8.5)

4.5.3   Inertia matrices and constant values

$I_{\text{com\_s}}, I_{\text{com\_d}}, I_{\text{com\_e}}$, and $I_{\text{com\_p}}$ are the inertia matrices for the sphere, differential, electronics, and pendulum systems, respectively.

$I_{\text{com\_s\_11}}, I_{\text{com\_s\_22}}, I_{\text{com\_s\_33}}, I_{\text{com\_d\_11}}, ..., I_{\text{com\_p\_33}}$ represent the diagonal elements of each inertia matrix.

$$
I_{\text{com\_s}} = \begin{bmatrix} I_{\text{com\_s\_11}} & 0 & 0 \\ 0 & I_{\text{com\_s\_22}} & 0 \\ 0 & 0 & I_{\text{com\_s\_33}} \end{bmatrix}, \tag{4.41}
$$

$$
I_{\text{com\_d}} = \begin{bmatrix} I_{\text{com\_d\_11}} & 0 & 0 \\ 0 & I_{\text{com\_d\_22}} & 0 \\ 0 & 0 & I_{\text{com\_d\_33}} \end{bmatrix}, \tag{4.42}
$$

$$
I_{\text{com\_e}} = \begin{bmatrix} I_{\text{com\_e\_11}} & 0 & 0 \\ 0 & I_{\text{com\_e\_22}} & 0 \\ 0 & 0 & I_{\text{com\_e\_33}} \end{bmatrix}, \tag{4.43}
$$

$$
I_{\text{com\_p}} = \begin{bmatrix} I_{\text{com\_p\_11}} & 0 & 0 \\ 0 & I_{\text{com\_p\_22}} & 0 \\ 0 & 0 & I_{\text{com\_p\_33}} \end{bmatrix}. \tag{4.44}
$$

Parameter	Value (SI)
Radius (R)	0.25
Combined Length (le)	$\frac{34.6+31}{1000}$
Pendulum Length (lp)	$\frac{133.643612}{1000}$
Electronics Mass (M_e)	1
Differential Mass (M_{diff})	1.78945
Pendulum Mass (M_p)	15.44337
Sphere Mass (M_{sf})	3.65323
Sphere Inertia Matrix ($I_{\text{com\_sf}}$)	$I_{\text{com\_sf\_11}} = \frac{139440674.62}{10^9}$ $I_{\text{com\_sf\_22}} = \frac{114230485.45}{10^9}$ $I_{\text{com\_sf\_33}} = \frac{139459059.83}{10^9}$
Differential Inertia Matrix ($I_{\text{com\_diff}}$)	$I_{\text{com\_diff\_11}} = \frac{1868420.801851}{10^9}$ $I_{\text{com\_diff\_22}} = \frac{9453074.272454}{10^9}$ $I_{\text{com\_diff\_33}} = \frac{10584618.029037}{10^9}$
Electronics Inertia Matrix ($I_{\text{com\_e}}$)	$I_{\text{com\_e\_11}} = \frac{2551039.209892}{10^9}$ $I_{\text{com\_e\_22}} = \frac{6465944.705112}{10^9}$ $I_{\text{com\_e\_33}} = \frac{7588376.182422}{10^9}$
Pendulum Inertia Matrix ($I_{\text{com\_p}}$)	$I_{\text{com\_p\_11}} = \frac{118358255.573059}{10^9}$ $I_{\text{com\_p\_22}} = \frac{88903297.974851}{10^9}$ $I_{\text{com\_p\_33}} = \frac{149463371.597378}{10^9}$
Acceleration due to Gravity (g)	9.80665

Table 4.1: Parameter Values

4.5.4 Lagrangian Definition

L'equazione Lagrangiana L è definita come L = K - T

Define kinetic energies

$$K_{\text{sf}} = \frac{1}{2}M_{\text{sf}}\left(v_s'\right)^T v_s + \frac{1}{2}w_s^T I_{\text{com\_s}} w_s; \tag{4.45}$$

$$K_{\text{diff}} = \frac{1}{2}M_{\text{diff}}(v_d)'v_d + \frac{1}{2}w_d^T I_{\text{com\_d}} w_d; \tag{4.46}$$

$$K_{\text{e}} = \frac{1}{2}M_{\text{e}}(v_e)'v_e + \frac{1}{2}w_e^T I_{\text{com\_e}} w_e; \tag{4.47}$$

$$K_{\text{p}} = \frac{1}{2}M_{\text{p}}(v_p)'v_p + \frac{1}{2}w_p^T I_{\text{com\_p}} w_p; \tag{4.48}$$

$$K = K_{\text{p}} + K_{\text{e}} + K_{\text{diff}} + K_{\text{sf}}; \tag{4.49}$$

Define potential energies

$$P_{\text{sf}} = M_{\text{sf}} \cdot g \cdot p_s(3); \tag{4.50}$$

$$P_{\text{diff}} = M_{\text{diff}} \cdot g \cdot p_d(3); \tag{4.51}$$

$$P_{\text{e}} = M_{\text{e}} \cdot g \cdot p_e(3); \tag{4.52}$$

$$P_{\text{p}} = M_{\text{p}} \cdot g \cdot p_p(3); \tag{4.53}$$

$$P = P_{\text{p}} + P_{\text{e}} + P_{\text{diff}} + P_{\text{sf}}; \tag{4.54}$$

The generalized Lagrange equation with constraints is given by:

$$\frac{d}{dt}\left(\frac{\partial L}{\partial \dot{q}_i}\right) - \frac{\partial L}{\partial q_i} = Q_i + \sum_j \lambda_j \frac{\partial \phi_j}{\partial q_i} \tag{4.55}$$

where:

- L is the Lagrangian of the system, defined as $L = K - P$, where K is the kinetic energy and P is the potential energy.

- $\dot{q}_i$ are the generalized velocities.

- Q_i are the generalized forces acting on the system.

- λ_j are the Lagrange multipliers associated with the constraints $\phi_j(q_1, q_2, \ldots, q_n, t) = 0$.

- ϕ_j are the constraint equations which may depend on the generalized coordinates, time, and parameters.

This equation represent the dynamics with the effects of both applied and internal forces, incorporating the non-holonomic constraints.

4.5.5 Dynamics equation and tests

The dynamic equation of the system is given by:

$$M \cdot \ddot{q} + V = A^T \cdot \lambda + E \cdot u \tag{4.56}$$

The input vector u is defined as:

$$u = \begin{bmatrix} \tau_1 \\ \tau_2 \end{bmatrix} \tag{4.57}$$

The matrix E is defined as:

$$E = \begin{bmatrix} 0 & 0 \\ 0 & 0 \\ 0 & 0 \\ 0 & 0 \\ 0 & 0 \\ 1 & 0 \\ 0 & 1 \end{bmatrix} \tag{4.58}$$

Non-holonomic constraint

The constraints in the Lagrange equation are represented by the matrices λ, A, and C:

$$\lambda = \begin{bmatrix} \lambda_1 \\ \lambda_2 \\ \lambda_3 \end{bmatrix} \tag{4.59}$$

λ is the vector of Lagrange multipliers associated with the constraints.

$$A = \begin{bmatrix} 1 & 0 & 0 & -R\cos(\theta_z) & -R\cos(\theta_y)\sin(\theta_z) & 0 & 0 \\ 0 & 1 & 0 & -R\sin(\theta_z) & R\cos(\theta_y)\cos(\theta_z) & 0 & 0 \\ 0 & 0 & 1 & 0 & -\sin(\theta_y) & 0 & 0 \end{bmatrix} \quad (4.60)$$

A is the constraint matrix that depends on the generalized coordinates q_i.

The matrix C represents the null space (kernel) of A:

$$C = \text{null}(A) \quad (4.61)$$

C consists of a matrix that satisfy the equation $AC = 0$.

These matrices are essential for formulating the Lagrange equation, in systems where constraints restrict the motion of generalized coordinates q_i.

C matrix is then multiplied to both equation member, this lead to the simplification of the constraint quantity.

The generalized variables are separated into $\boldsymbol{q}_1$ and $\boldsymbol{q}_2$. The corresponding velocity vectors $\dot{\boldsymbol{q}}_1$, $\dot{\boldsymbol{q}}_2$ and acceleration $\ddot{\boldsymbol{q}}_2$ are the following:

$$\dot{\boldsymbol{q}}_1 = \begin{bmatrix} \dot{x} \\ \dot{y} \\ \dot{\theta}_z \end{bmatrix} \quad \dot{\boldsymbol{q}}_2 = \begin{bmatrix} \dot{\theta}_y \\ \dot{\theta}_x \\ \dot{\alpha} \\ \dot{\beta} \end{bmatrix} \quad \ddot{\boldsymbol{q}}_2 = \begin{bmatrix} \ddot{\theta}_y \\ \ddot{\theta}_x \\ \ddot{\alpha} \\ \ddot{\beta} \end{bmatrix} \quad (4.62)$$

The relation between $\dot{\boldsymbol{q}}_1$ e $\dot{\boldsymbol{q}}_2$ is the following:

$$\dot{\boldsymbol{q}}_1 = -\boldsymbol{A}_2 \dot{\boldsymbol{q}}_2 \quad (4.63)$$

Where $\boldsymbol{A}_2$ is defined as

$$\boldsymbol{A}_2 = \begin{bmatrix} -R\cos(\theta_z) & -R\cos(\theta_y)\sin(\theta_z) & 0 & 0 \\ -R\sin(\theta_z) & R\cos(\theta_y)\cos(\theta_z) & 0 & 0 \\ 0 & -\sin(\theta_y) & 0 & 0 \end{bmatrix} \quad (4.64)$$

and it is the right submatrix of matrix $\boldsymbol{A}$.

The entire system can be represented by the following equation:

$$\bar{M}_1 \ddot{q}_2 + \bar{M}_2 \dot{q}_2 + \bar{V} = \bar{I} u \tag{4.65}$$

where:

- $\ddot{q}_2$ are the generalized accelerations of q_2,

- $\dot{q}_2$ are the generalized velocities of q_2,

- u is the input force/moment vector,

- $\bar{M}_1$, $\bar{M}_2$, $\bar{V}$, e $\bar{I}$ are the derived Matrices/vectors.

In particular, as previously stated, to simplify the dynamics equation the C matrix has been multiplied to every equation member. The final derived matrices are defined as follows:

$$\bar{M}_1 = C^\top M C \tag{4.66}$$

$$\bar{M}_2 = C^\top M dC \tag{4.67}$$

$$\bar{V} = C^\top V \tag{4.68}$$

$$\bar{I} = C^\top E \tag{4.69}$$

Final form of dynamical equations present the shape below:

$$G_1 = \bar{M}_1 \ddot{q}_2 + \bar{M}_2 \dot{q}_2 + \bar{V} \tag{4.70}$$

$$G_2 = \bar{I} u \tag{4.71}$$

Chapter 5

Controller

5.1 Introduction

After generating the multibody model of the rover, in order to close the system control loop, the next steps are to model the sensors, add disturbances, and program a robust controller capable of following the imposed reference. The development of the controller was defined in multiple steps. The structure of a controller was already elaborated in previous works [2], and allowed to manipulate the rover for linear motion only. Following various tests and performance evaluations of the aforementioned straight controller, a lateral side stabilization controller was defined. The performance of this controller was assessed both independently and in conjunction with the linear controller. Finally, tests with different references for planar movement of the rover were conducted and the performance of the final control system was evaluated.

5.2 Straight path trajectory

5.2.1 Sensor data acquisition

As seen in Part 1 of the thesis, all the electronic components required to be integrated into the rover to obtain the necessary data for the control system have been defined. These include the two IMUs installed on the pendulum and the differential box, as well as the encoders on the main motors. The sensors are considered ideal, implying that measurements perfectly are noise-free reported to the controller. A structure

implementing a model with a more realistic representation is discussed in the Future Works chapter.

5.2.2 Fuzzy PID controller

Several challenges and problems arise when discussing about the problem of the rover to follow longitudinal trajectories. The first challenge is determining the nature of reference that the rover should follow. In this case, the aim is to develop a speed control system. A linear speed is defined as reference to achieve fot the center of the sphere. Error function is defined as the difference between the reference angular velocity of the sphere and the angular velocity computed using the differential formula 2.1, 2.2.

The controller elaborated in [2] is a Fuzzy PID controller, which computes the proportional, integrative, and derivative values to be set into a PID controller. The PID receives as input the numerical value of the calculated error.

A new tuning of the parameters has been performed to adapt the controller to the studied spherical rover.

In conclusion, to generate an input for the plant, the final input signal is the current value to be fed into the motor. Hence, the implementation of gain and saturation is necessary to transmit an input value that conforms to the plant limitations.

5.2.3 Tests and results

The types of tests considered include step reference signals, ramp signals, and signal generator inputs. Rover's transient phase response to these inputs was evaluated. Results for the forward controller fed by step input of $4rad/s$ are presented:
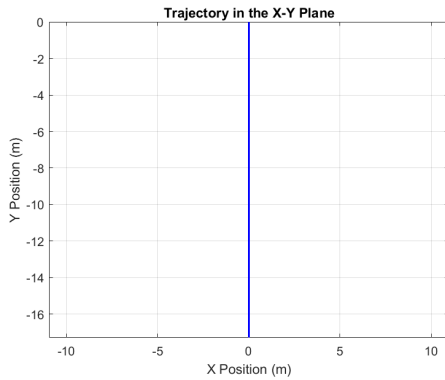
Figure 5.1: Followed trajectory
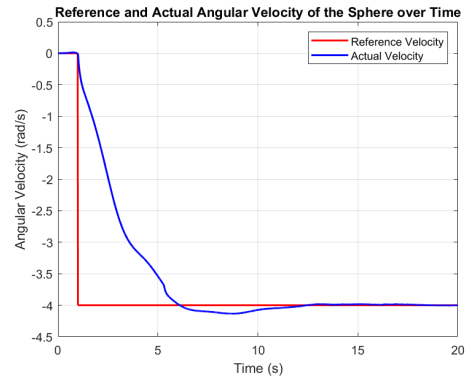
Figure 5.2: Linear Velocity reference tracking

Transient performances in Figure 5.2, are reported here below

	Rise Time	Settling Time 2%	Overshoot
STEP 1 m/s	5.09s	9s	3.25%

Table 5.1: Performance Metrics for STEP 1 m/s

Other tests were performed with other step input values. In particular, the table with the performance for tests conducted with step inputs of magnitude "-1" , "2.5" and "-2.5". Note that a speed of $2.5m/s$ was by construction defined as the desired nominal speed of the Spherical Rover.

	Rise Time	Settling Time 2%	Overshoot
STEP -1 m/s	5.09s	9s	3.25%
STEP 2.5 m/s	6.84s	10.02s	4.35%
STEP -2.5 m/s	//	//	//

Table 5.2: Performance Metrics for Various Steps

The final tests regarding the proposed controller ends with the performance evaluation for two kind of signals. The first one is showed in Figure5.3. Results exhibit a precise longitudinal trajectory, shown in Figure 5.4, and a signal tracking like presented in fig.5.5.

While the second test is executed setting the input in fig.5.6, also here longitudinal trajectory is achieved (fig. 5.7) and finally the figure5.8 shows the tracking performance.
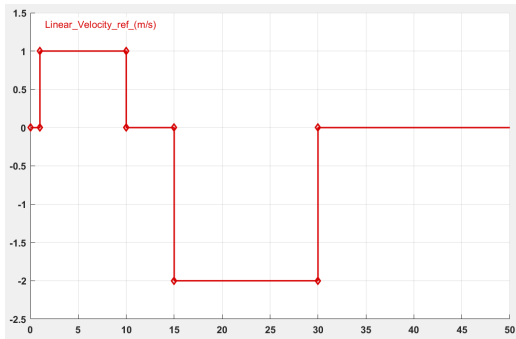
Figure 5.3: Signal step inputs
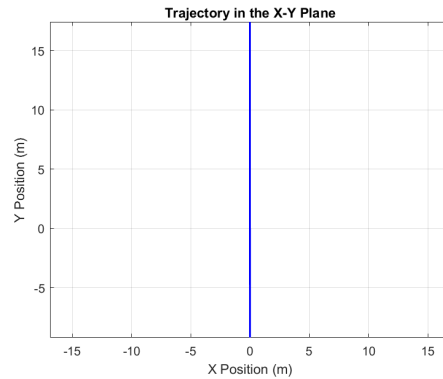
Figure 5.4: Step inputs Trajectory
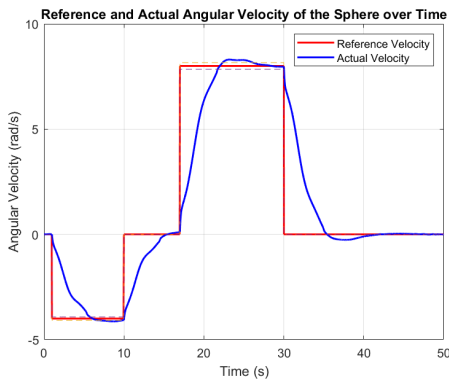
Figure 5.5: Reference tracking
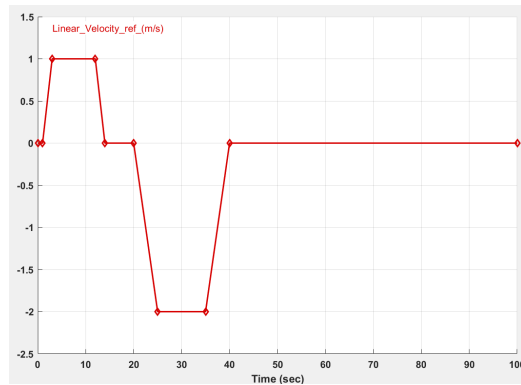
Figure 5.6: Signal ramp inputs
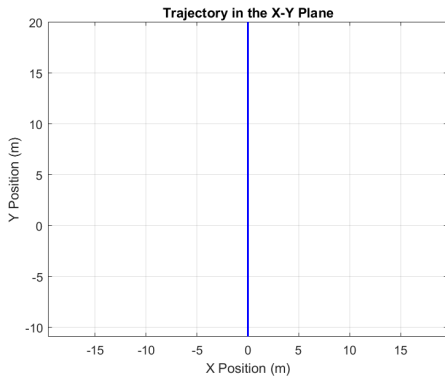
Figure 5.7: Ramp inputs Trajectory
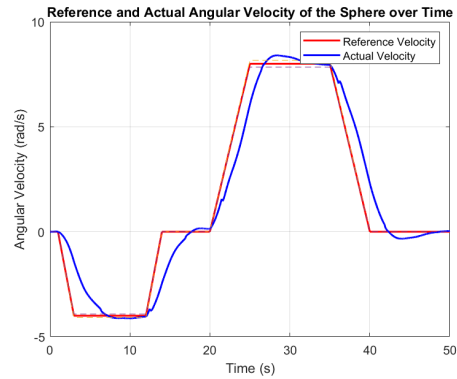
Figure 5.8: Reference tracking

Slope climbing

For this simulation we address the problem of evaluate the robot performance set on an inclined plane. Result are provided for different slope values, in particular 1° and 8°.

In this test we implement a 1° slope infinite plane, and the linear velocity reference of 1 m/s.

The robot as soon as the simulation start, it is not able to going forward and reach the wanted reference this because it present the Center of Mass shifted by a certain quantity. This behaviour is also related to all the slope simulations.

Result for trajectory, linear velocity tracking and general evaluation are shown in figure 5.11, 5.9, 5.10.
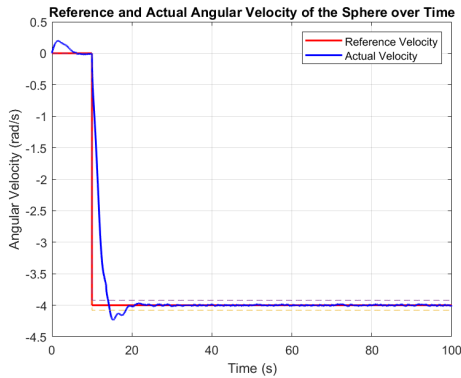
Figure 5.9: Linear velocity reference tracking
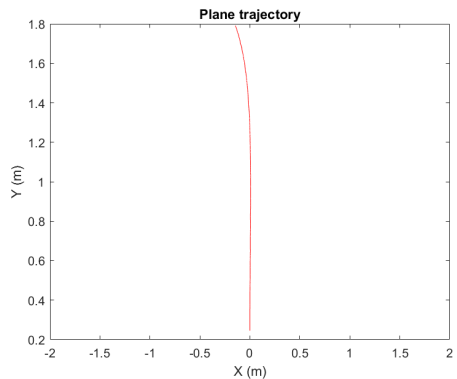
Figure 5.10: Trajectory

59
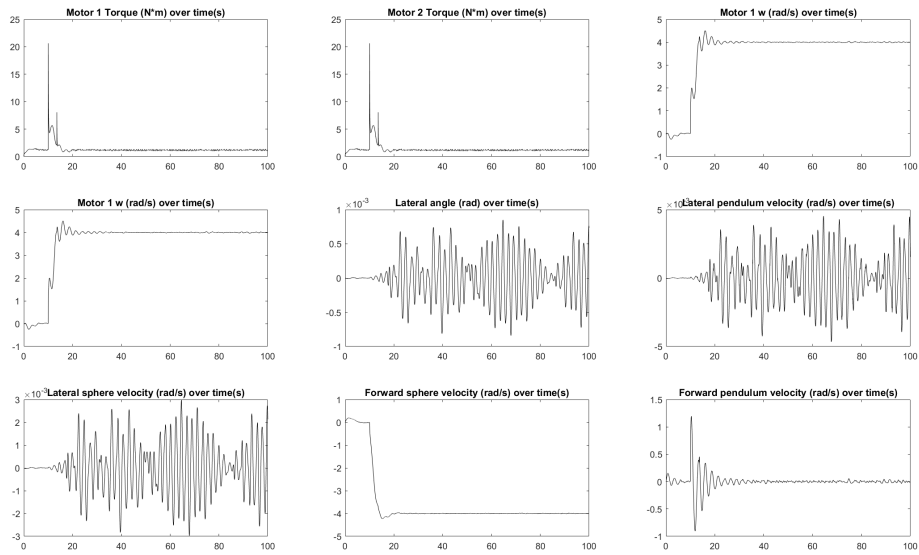
Figure 5.11: Overall evaluation

The next test has been made setting up an 8° plane slope. Test have been made for 0 linear velocity tracking. Results simulation plots are presented in figure 5.13,5.14,5.12,5.15.
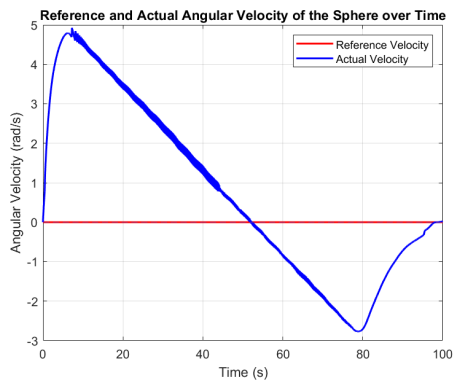
Figure 5.12: Reference tracking
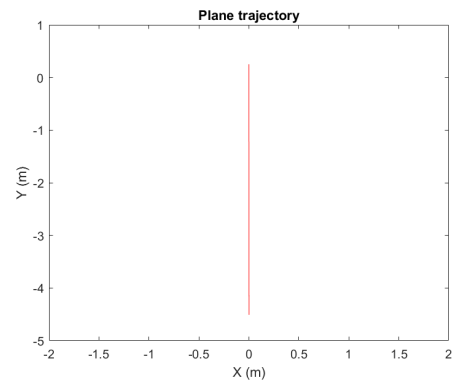
Figure 5.13: Trajectory
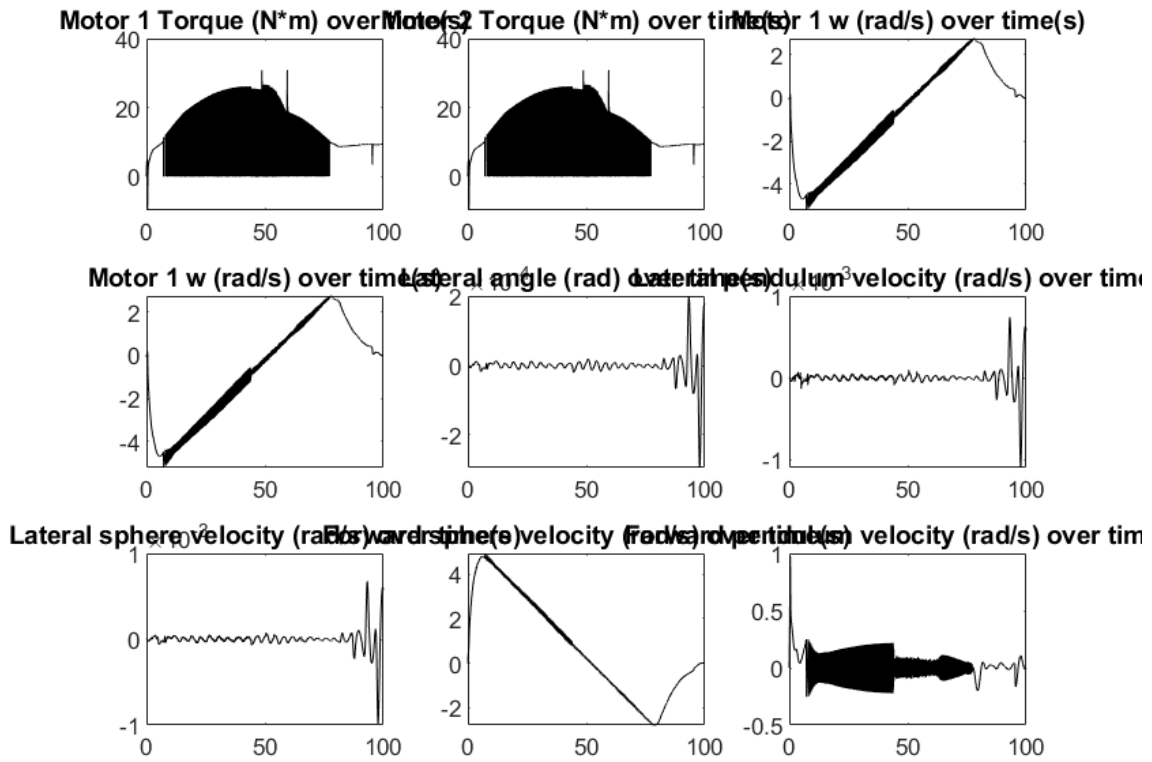
Figure 5.14: Overall evaluation
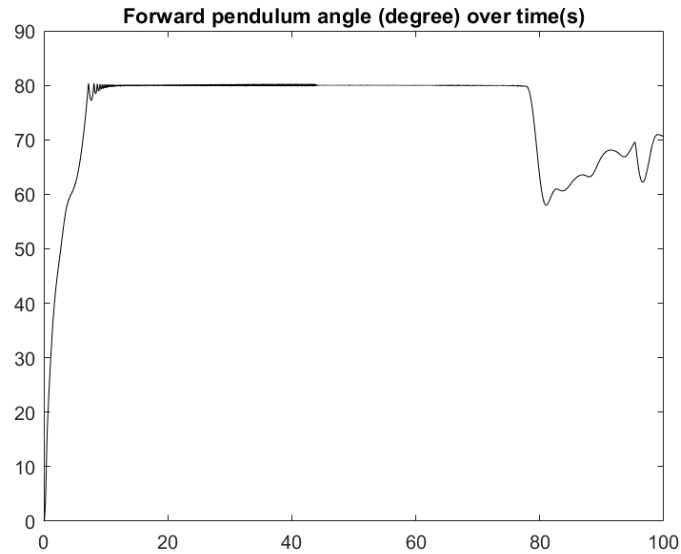
Figure 5.15: forward angle

It is possible to see that although a perfect linear trajectory, robot is constatly rolling backwards as the condition to reach 0 rad/s in a 8° slope plane is very challenging to it. In fact after around 95 seconds simulation the robot perform complete reference tracking. In addition from figure 5.15 the pendulum is constantly raised at 80° in order to overtake inertia forces. reached 0 sphere angular velocity, pendulum set to 70 degree to maintain still position.

Other test made, led to inconsistent result. The spherical rover is probably able to climb planes with higher slope ,thats because the resting angle achieved by the pendulum is around 70° and it can be at most 90°. At the contrary all the subsequent simulations, present a deviation to the straight trajectory, or the simulation takes to much to prove it.

5.3   Lateral side controller

5.3.1   Former problem

An initial approach to controlling the robot for planar trajectories involves focusing on the lateral angle control of the pendulum. To generate a curved trajectory, the internal

pendulum must maintain a specific angle relative to the main shaft. Additionally, the spherical shell must not exhibit lateral oscillations, as this would result in erratic and unstable movements of the rover. The main shaft must maintain an angle with the plane that is complementary to the angle with the pendulum. Thus, pendulum angle can be used for the determination of the rover's curvature radius.

5.3.2 Standstill controller

The controller Simulink scheme is represented in figure5.16
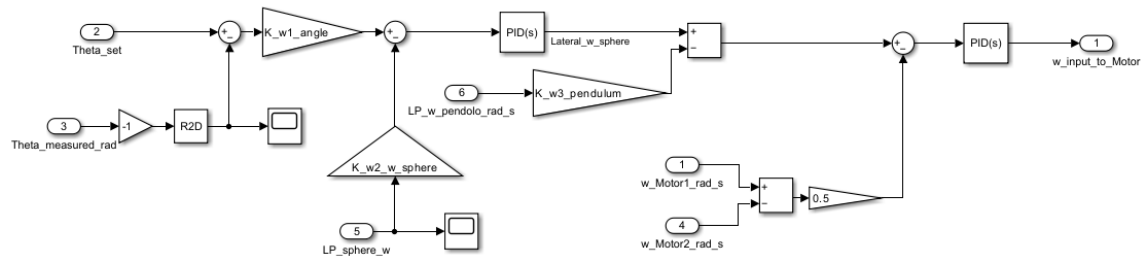
Figure 5.16: Lateral Controller

$$\theta \tag{5.1}$$

angle .

The purpose of this system is to set and track a reference input (θ_{set}). This angle correspond to the space portion between the pendulum and the main shaft.
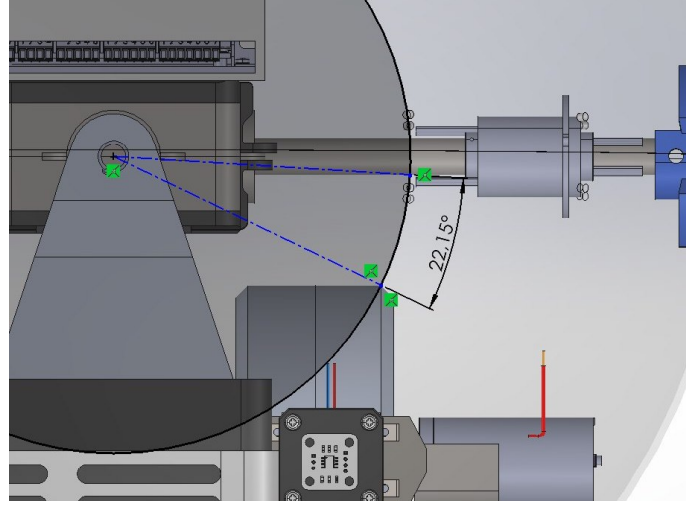
Figure 5.17: Maximum lateral angle

An error function e_θ is computed by subtracting the measured angle $\theta_{measured}$ from the reference angle θ_{set}. The measured angle, in radians (rad), is converted into degree through the Simulink block R2D for a more intuitive implementation of the control strategy.

The angle is measured by the IMU sensor. Either, the same data could be obtained through the integration of the angular velocity detected by the an encoder.

The angular error is amplified by a gain K_{w1} and then passed through a PID controller to generate the corrective command needed to reduce the error.

This signal is considered as

$$\Omega_{\text{sphere}}$$

Then the sphere angular speed Ω_{sphere} and the pendulum speed $\Omega_{pendulum}$ are then weighted by coefficient K_{w2} e K_{w3}.

The control action is based on the relation:

$$\Omega_{pendulum} + \Omega_{sphere} = \frac{w_{motor1} + w_{motor2}}{2}$$

Since the signal of w_{motor2} measured by the plant is negative, the minus sign is inserted into the "sum" block of Simulink.

The output signal of the PID controller is summed with the compensated signals of the ball and pendulum velocity to generate the total command needed to follow the

reference angle.

The total control signal is then passed through an additional PID controller to generate the final command $w_{InputToMotor}$, which is the input to be provided to the robot's motors.

The angular velocities of the two motors (w_{Motor1} and w_{Motor2}) are summed and amplified to generate a feedback signal. This feedback is compared with the total command of the PID controller to ensure that the motors follow the desired command. The control system described is designed to ensure that the robot follows the reference angle (θ_{set}) accurately, minimizing error and compensating for the angular velocities of the sphere and pendulum. This integrated approach ensures stable and precise control of the robot's motion.

5.3.3 Test

Next step consist of simulating the closed-loop control by inserting an input constant reference of 10°. Results are reported here regarding the transient behaviour. An important parameter to check is the oscillation of the sphere and after how long it stabilizes or reaches a settling time.

Table 5.3 fig. 5.18 5.19 5.20

	Rise Time	Settling Time 2%	Overshoot
STEP 10°	5.09s	9s	3.25%
STEP -10°	//	//	//

Table 5.3: Performance Metrics for STEP 1 m/s
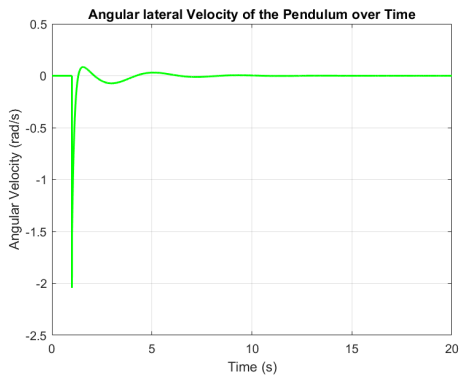
Figure 5.18: Pendulum angular velocity
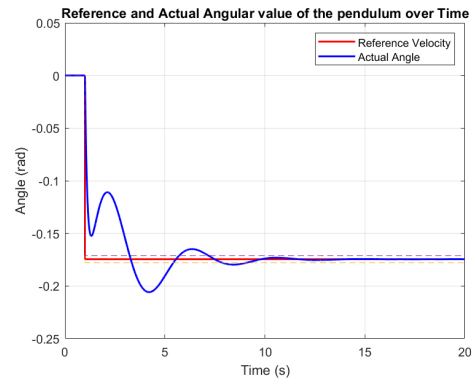
Figure 5.19: Lateral angle tracking
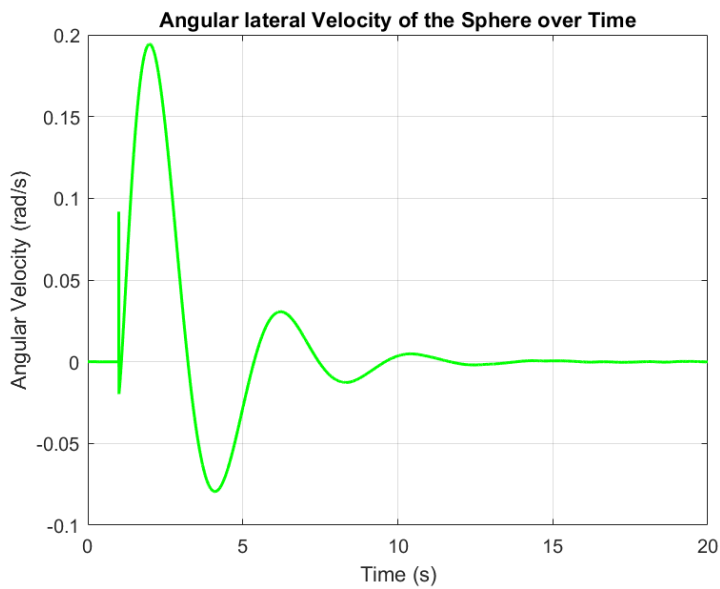
Figure 5.20: Lateral sphere angular velocity

Further tests were performed considering a signal as showed in figure 5.21 , it is composed of several steps, in which we can discuss about the Rover reference tracking behaviour in the simulations in figure5.22 5.23 5.24
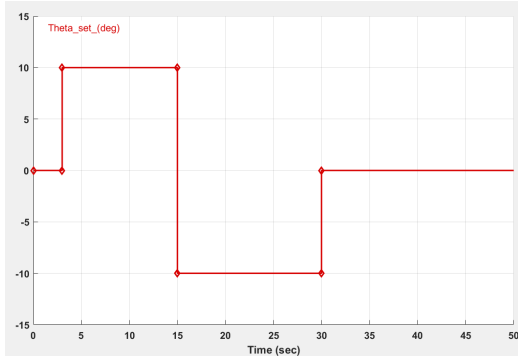
Figure 5.21: Input
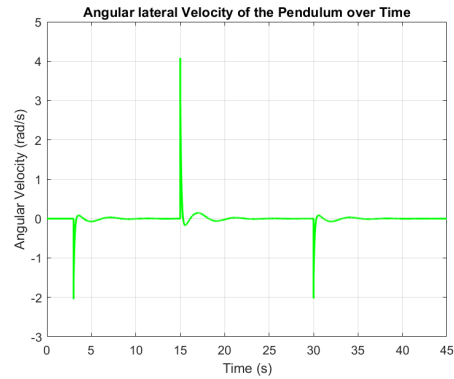
Figure 5.22: Lateral pendulum angular velocity
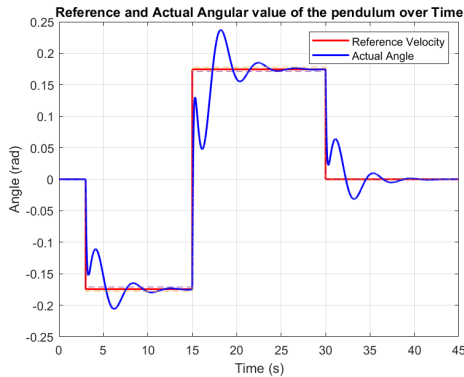
Figure 5.23: Lateral Angle tracking
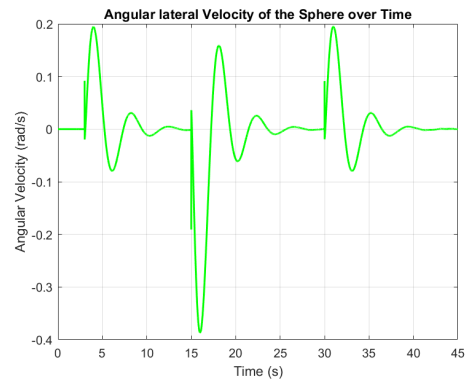
Figure 5.24: Lateral sphere angular velocity

Considering the results obtained from the tests performed, a slow transient trend can be seen, taking into consideration the settling and rise time values. This is considered preferable in order to remain prudent and obtain appreciable stabilization especially of the lateral angular velocity of the sphere, which is very important in curved trajectories.

5.4 Plane trajectories

To achieve a control over curved trajectories, the concepts previously studied are combined and a unique controller is formalized.
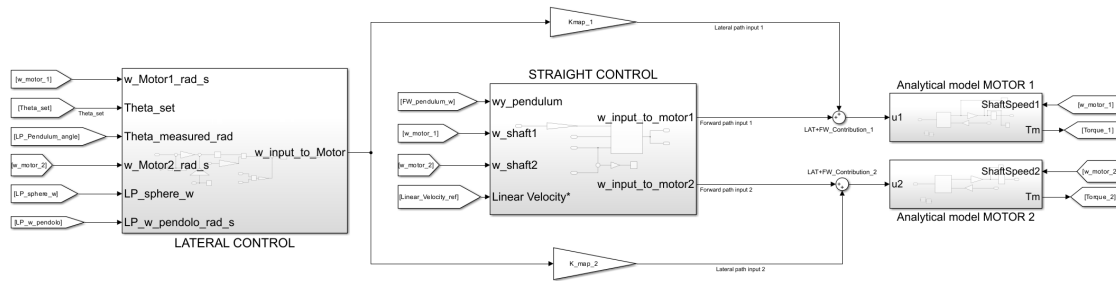
Figure 5.25: Complete controller

As can be seen from the figure 5.25 the output signals from both, Lateral and Straight controllers, are fed into the "sum" blocks and the output values ("u1" and "u2") sent to the pendulum motor schematization i.e. "Analytical model MOTOR 1" and "Analytical model MOTOR 2"

Throughout various simulations, the performance of the developed controller under different reference and territory conditions is shown in the next section.

5.4.1 Circular trajectory

Below is reported the controller that combines a longitudinal and lateral trajectory to obtain a planar path and execute curves with a given radius of curvature

The control was tested for 100s of simulation by entering 2 specific references for linear sphere velocity and pendulum angle i.e., 2 step inputs of, respectively, -1m/s and -10°. The simulations that follow show a circular trajectory with radius of about 9m a good stabilization of the lateral angle visible in figure 5.27,
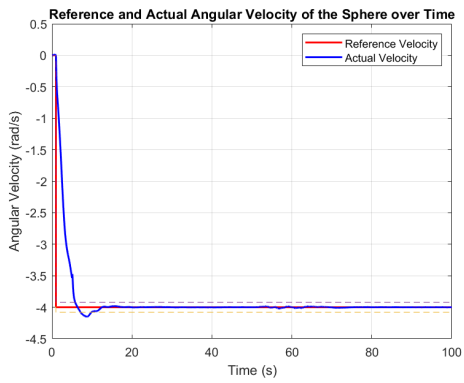
Figure 5.26: FW sphere angular velocity
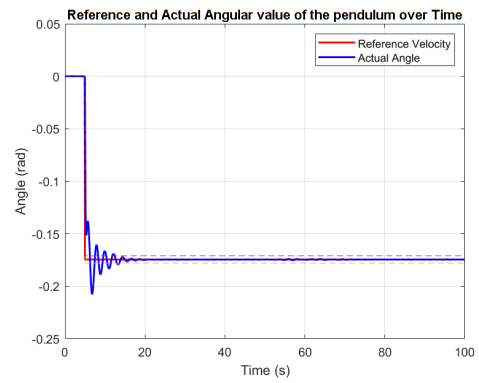
Figure 5.27: Lateral pendulum angle tracking
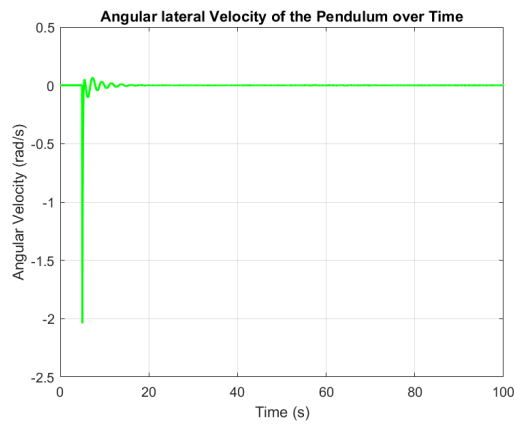
Figure 5.28: Lateral pendulum angular velocity
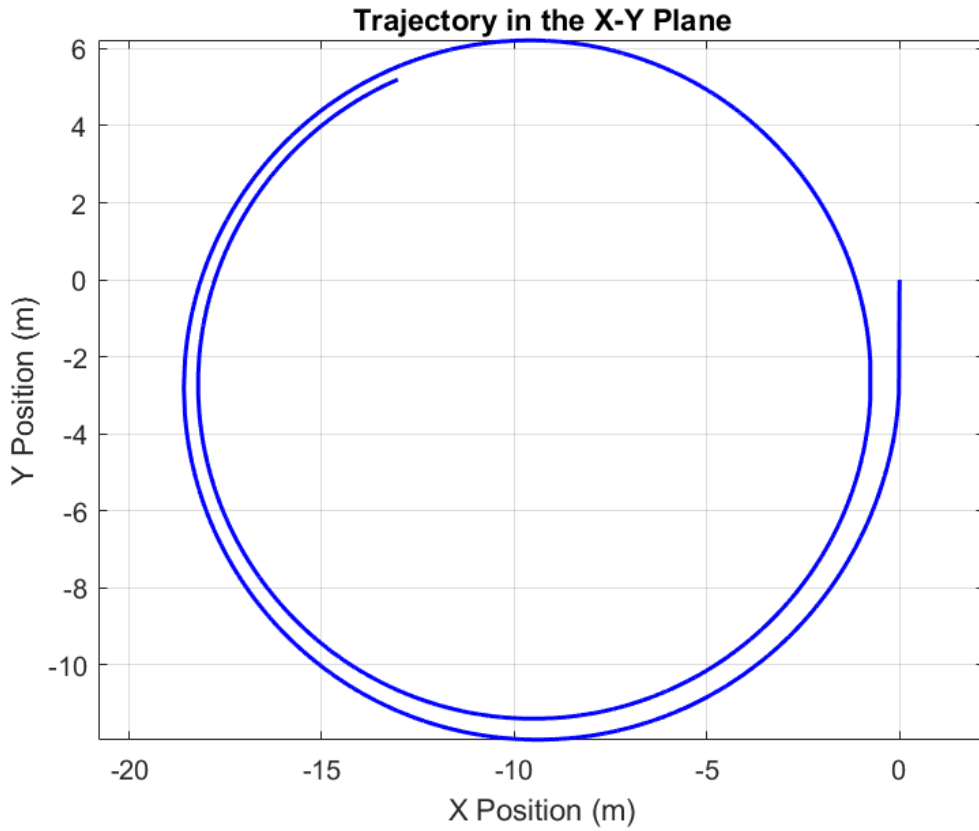
Figure 5.29: Plane trajectory
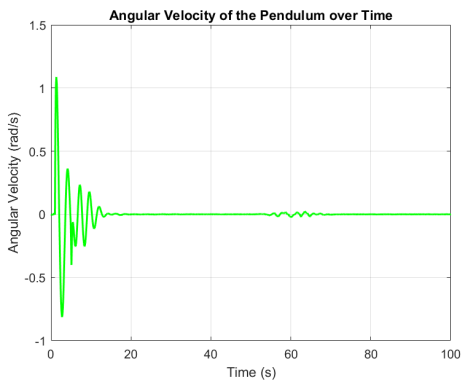
Figure 5.30: Pendulum angular velocity
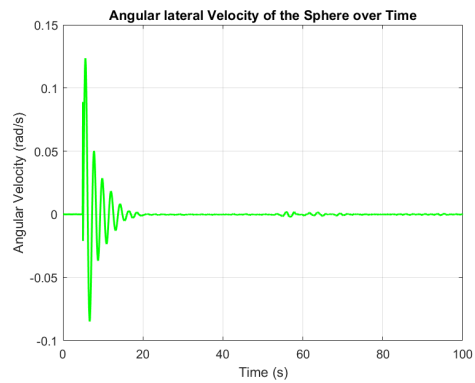
Figure 5.31: Lateral sphere angular velocity

As shown in the previous simulations, the controlled Rover present the following results:

- Pendulum angular velocity along x-axis (lateral axis) (forward navigation) stabilization after around 17 seconds and smooth behaviour, fig.5.30

- Lateral angular sphere velocity i.e. around z-axis, stabilization and so the sphere is not oscillating while performing the reference tracking fig.5.31

- Trajectory following with a good reliability, it has seen an error of 0.5m during a 9m radii of circular trajectory fig.5.29

- Reference tracking for both Lateral angle Θ and linear velocity fig.5.26,fig,5.27

Step climbing

In this part, is presented a test phase for evaluating the maximum step high that the robot is able to overcome. This argument is widely discussed and presented in [2]. Note that Rover design has been changed it lead to different mass, COM and inertia. For this reason they show different performances.

After several simulation by SimMechanics, the rover perform a maximum step high of 22mm. The presented result is reported after a test close to standstill condition. Robot velocity has been set to $2m/s$ that is $8rad/s$, step is positioned right in front of the sphere. Step is represented as a cylindrical mass positioned at the wanted high. Results are also showed in figure 5.32, 5.33. Step is position right after the sphere. The Rover overcome it at second 11 and most important to take in consideration is the pendulum angle, it is constantly around 90° degree that is the maximum condition to have COM distant from center of the sphere, this is the condition to impose in order to present the maximum performance of the rover.
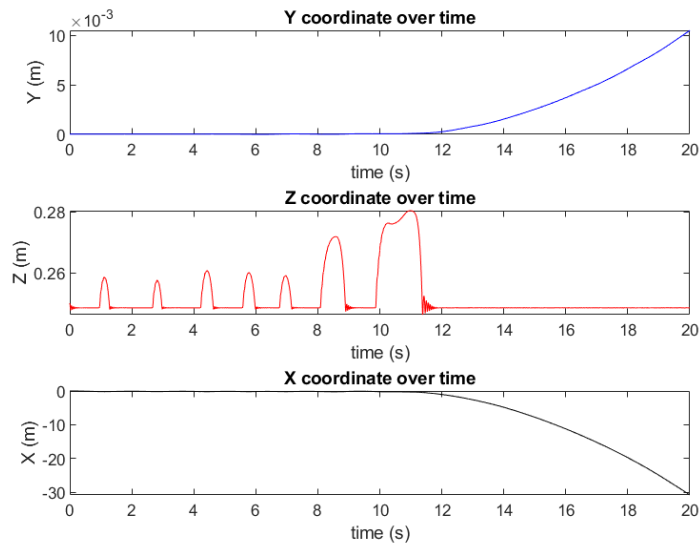
Figure 5.32: Trajectory
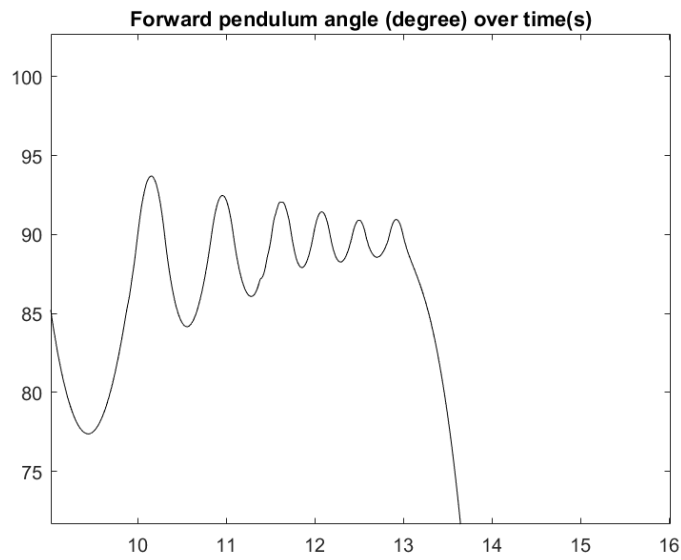
Figure 5.33: Forward angle

It is important to mention that the robot is able to overcome higher steps if only inertia is considered. More important to say is that CMG devices provide a boost action to the sphere with a maximum torque of 25.42, hence the activation of the

CMG system lead to climb slope planes and steps bigger than the result presented but only for few seconds a the provided torque is instantly and not continuously provided.

Chapter 6

Results

In this chapter, we present the results achieved throughout the development and testing phases of the spherical robot. The outcomes are organized based on the different aspects and chapters of the project.

6.1   Performance Analysis

One of the significant achievements in the performance analysis chapter is determining the operational endurance of the robot. By selecting an appropriate battery, we have ensured that the robot can operate continuously for 1 hour. This operational time was calculated under the assumption of continuous usage, making the robot suitable for extended tasks without frequent recharging.

Additionally, we verified that the selected battery and power system can generate the necessary current to drive the motors, especially during maneuvers involving the two Control Moment Gyroscopes (CMGs). The system can handle the intense load required for these maneuvers, ensuring stable and reliable performance.

6.2   Plant Definition

In the plant definition chapter, we developed two multibody models for the robot in Simulink. The first is a high-fidelity model that provides an accurate representation of the robot's dynamics and behavior. This model is essential for detailed analysis

and validation.

The second model is a simplified version, which significantly reduces the simulation time while maintaining performance accuracy. This model is particularly useful for iterative design and testing processes where quick feedback is essential.

The third one, as discussed by the simulation behaviour, performance differ too much from the first and second one and so, debug and adjustment need to be done in order to validating it.

6.3 Controller Development

The developed controller has demonstrated good performance in response to various reference signals, including step inputs, ramp signals, and generated signal profiles. The controller's ability to accurately follow these reference signals indicates robust performance and reliability.

Joypad control is also possible to implement, for input generation during real-time simulations.

Furthermore, the controller enables the robot to generate and follow curved trajectories with high reliability. However, it is essential to note that the trajectories are subject to a minimum curvature radius. The controller cannot generate trajectories with a curvature radius smaller than 0.68 m, which is a limitation to be addressed in future work.

Overall, the results indicate that the spherical robot with an internal pendulum meets the design and performance criteria set out at the beginning of the project. The developed models and controller provide a solid foundation for further enhancements and practical implementations.

Chapter 7

Feature Works

7.1   Introduction

This chapter discusses possible future extensions and improvements to the work presented in this thesis. Areas identified for future development include virtual sensor modeling, control system testing, implementation of trajectory planning and obstacle avoidance algorithms, gyroscope testing, and assembly of the robot with real components.

7.2   Virtual sensors modelling

One of the most important direction for future model a more robust system is the implementation of virtual sensor modeling on Simulink. This approach allow:

- Realistically model sensor errors, including systematic and random errors.

- To test the effectiveness of the controller developed in the thesis by evaluating its robustness against sensor errors.

- Develop a more robust controller that accounts for sensor errors to improve system performance.

7.3 Control system test with virtual microcontroller

Another important step is the transition to the Software-in-the-Loop (SIL) phase, which involves:

- Use a virtual microcontroller to test the control system, simulating the real execution environment.

- Assess the compatibility of the control code with the intended hardware and identify any integration issues.

7.4 Implementation of trajectory algorithm and obstacle avoidance function

Using the formulas of dynamics derived throughout this thesis, it is possible:

- Implement a controller using direct and inverse dynamics for robot trajectory planning.

- Develop obstacle avoidance algorithms that enable the robot to navigate complex environments.

7.5 Gyroscopes tests

Further testing of gyroscopes is needed to:

- Evaluate the accuracy and reliability of the data provided by the gyroscopes during robot movement.

- Calibrate the gyroscopes to reduce errors and improve the overall performance of the control system.

Additionally,a mention about the electronics positioning need to be discussed. The electronics physical system is located into the electronics box, placed above the

differential box. That spot, although represent the best solution to maintain a symmetric COM and an organized electronics system, it is highly counterproductive. The weight in the position produce an upper lifting of the ROV COM. This lead to reduced performance. It is possible to try to reposition the electronics system in order to enhance the Rover performance and also to keep easy access and easy cabling. Finally, a crucial step is the purchase of all the components discussed and the assembly of the robot so as to make the first prototype and apply all the theoretical studies and insights made. The physical assembly of the robot has to be followed by a series of tests to verify the proper functioning of the integrated system.

Chapter 8

Appendix

Linear velocity of the electronics box

$$
\mathbf{v}_e = \begin{bmatrix} dx - le \cdot (\sin(\alpha) \cdot d\alpha \cdot (\sin(\theta_x) \cdot \sin(\theta_z) + \cos(\theta_x) \cdot \cos(\theta_z) \cdot \sin(\theta_y))) \\ le \cdot (\cos(\alpha) \cdot (\sin(\theta_x) \cdot \sin(\theta_z) \cdot d\theta_z - \cos(\theta_x) \cdot \cos(\theta_z) \cdot d\theta_x + \cos(\theta_x) \cdot \cos(\theta_y) \cdot \sin(\theta_z) \cdot d\theta_y + \cos(\theta_x) \cdot \cos(\theta_z) \cdot \sin(\theta_y) \cdot d\theta_z - \sin(\theta_x) \cdot \sin(\theta_y) \cdot \sin(\theta_z) \cdot d\theta_x)) \\ dy - le \cdot (\cos(\alpha) \cdot \sin(\theta_y) \cdot d\alpha + \sin(\alpha) \cdot \cos(\theta_y) \cdot d\theta_y + \cos(\alpha) \cdot \cos(\theta_y) \cdot \sin(\theta_x) \cdot d\theta_x + \cos(\alpha) \cdot \cos(\theta_x) \cdot \sin(\theta_y) \cdot d\theta_y + \sin(\alpha) \cdot \cos(\theta_x) \cdot \cos(\theta_y) \cdot d\alpha) \end{bmatrix}
$$

$$(8.1)$$

Linear velocity of the pendulum

$$
\mathbf{v}_p = \begin{bmatrix} dx - lp \cdot (\cos(\beta) \cdot \cos(\theta_x) \cdot \sin(\theta_z) \cdot d\beta - lp \cdot \sin(\beta) \cdot \cos(\theta_x) \cdot \cos(\theta_z) \cdot d\theta_z + lp \cdot \sin(\beta) \cdot \sin(\theta_x) \cdot \sin(\theta_z) \cdot d\theta_x \\ dy + lp \cdot (\cos(\beta) \cdot \cos(\theta_x) \cdot \cos(\theta_z) \cdot d\beta - lp \cdot \sin(\beta) \cdot \cos(\theta_z) \cdot \sin(\theta_x) \cdot d\theta_x - lp \cdot \sin(\beta) \cdot \cos(\theta_x) \cdot \sin(\theta_z) \cdot d\theta_z \\ lp \cdot (\cos(\beta) \cdot (\cos(\alpha) \cdot \sin(\theta_y) \cdot d\alpha + \sin(\alpha) \cdot \cos(\theta_y) \cdot d\theta_y + \cos(\alpha) \cdot \cos(\theta_y) \cdot \sin(\theta_x) \cdot d\theta_x + \cos(\alpha) \cdot \cos(\theta_x) \cdot \sin(\theta_y) \cdot d\theta_y + \sin(\alpha) \cdot \cos(\theta_x) \cdot \cos(\theta_y) \cdot d\alpha) \end{bmatrix}
$$

$$(8.2)$$

Angular velocity of sphere system

$$
\mathbf{w}_s = \begin{bmatrix} -\cos(\theta_z) \sin(\theta_y) \cdot d\theta_y - \cos(\theta_y) \sin(\theta_z) \cdot d\theta_z \\ \sin(\theta_x) \sin(\theta_z) \cdot d\theta_x - \cos(\theta_x) \cos(\theta_z) \cdot d\theta_z + \cos(\theta_x) \cos(\theta_z) \sin(\theta_y) \cdot d\theta_x + \cos(\theta_y) \cos(\theta_z) \sin(\theta_x) \cdot d\theta_y - \sin(\theta_x) \sin(\theta_y) \sin(\theta_z) \cdot d\theta_z \\ \cos(\theta_x) \sin(\theta_z) \cdot d\theta_x + \cos(\theta_z) \sin(\theta_x) \cdot d\theta_z + \cos(\theta_x) \cos(\theta_y) \cos(\theta_z) \cdot d\theta_y - \cos(\theta_z) \sin(\theta_x) \sin(\theta_y) \cdot d\theta_x - \cos(\theta_x) \sin(\theta_y) \sin(\theta_z) \cdot d\theta_z \end{bmatrix}
$$

$$(8.3)$$

Angular velocity of differential and electronics system

$$\mathbf{w}_d = \begin{bmatrix} -\sin(\alpha) \cdot (\cos(\theta_x)\sin(\theta_z) \cdot d\theta_x + \cos(\theta_z)\sin(\theta_x) \cdot d\theta_z + \cos(\theta_x)\cos(\theta_y)\cos(\theta_z) \cdot d\theta_y - \cos(\theta_z)\sin(\theta_x)\sin(\theta_y) \cdot d\theta_x - \cos(\theta_x)\sin(\theta_y)\sin(\theta_z) \cdot d\theta_z) \\ \sin(\theta_x)\sin(\theta_z) \cdot d\theta_x - \cos(\theta_x)\cos(\theta_z) \cdot d\theta_z + \cos(\theta_x)\cos(\theta_z)\sin(\theta_y) \cdot d\theta_x + \cos(\theta_y)\cos(\theta_z)\sin(\theta_x) \cdot d\theta_y - \sin(\theta_x)\sin(\theta_y)\sin(\theta_z) \cdot d\theta_z \\ \cos(\alpha) \cdot (\cos(\theta_x)\sin(\theta_z) \cdot d\theta_x + \cos(\theta_z)\sin(\theta_x) \cdot d\theta_z + \cos(\theta_x)\cos(\theta_y)\cos(\theta_z) \cdot d\theta_y - \cos(\theta_z)\sin(\theta_x)\sin(\theta_y) \cdot d\theta_x - \cos(\theta_x)\sin(\theta_y)\sin(\theta_z) \cdot d\theta_z) \end{bmatrix} \quad (8.4)$$

Angular velocity of pendulum system

$$\mathbf{w}_p = \begin{bmatrix} -\sin(\alpha) \cdot (\cos(\theta_x)\sin(\theta_z) \cdot d\theta_x + \cos(\theta_z)\sin(\theta_x) \cdot d\theta_z + \cos(\theta_x)\cos(\theta_y)\cos(\theta_z) \cdot d\theta_y - \cos(\theta_z)\sin(\theta_x)\sin(\theta_y) \cdot d\theta_x - \cos(\theta_x)\sin(\theta_y)\sin(\theta_z) \cdot d\theta_z) \\ \cos(\beta) \cdot (\sin(\theta_x)\sin(\theta_z) \cdot d\theta_x - \cos(\theta_x)\cos(\theta_z) \cdot d\theta_z + \cos(\theta_x)\cos(\theta_z)\sin(\theta_y) \cdot d\theta_x + \cos(\theta_y)\cos(\theta_z)\sin(\theta_x) \cdot d\theta_y - \sin(\theta_x)\sin(\theta_y)\sin(\theta_z) \cdot d\theta_z) \\ \cos(\beta) \cdot (\cos(\theta_x)\sin(\theta_y)\sin(\theta_z) \cdot d\theta_x - \cos(\theta_x)\sin(\theta_z) \cdot d\theta_z - \cos(\theta_z)\sin(\theta_x) \cdot d\theta_x + \cos(\theta_y)\sin(\theta_x)\sin(\theta_z) \cdot d\theta_y + \cos(\theta_z)\sin(\theta_x)\sin(\theta_y) \cdot d\theta_z) \end{bmatrix} \quad (8.5)$$

$$\begin{cases} dx = R \cdot \dot{\theta}_y \cdot \cos(\theta_z) + R \cdot \dot{\theta}_x \cdot \cos(\theta_y) \cdot \sin(\theta_z) \\ dy = R \cdot \dot{\theta}_y \cdot \sin(\theta_z) - R \cdot \dot{\theta}_x \cdot \cos(\theta_y) \cdot \cos(\theta_z) \\ d\theta_z = \dot{\theta}_x \cdot \sin(\theta_y) \end{cases} \quad (8.6)$$

DATA		
m_P	$16kg$	Pendulum estimated mass
L_P	$0.12m$	Pendulum estimated barycenter distance
τ_G	$25.82Nm$	Maximum gyroscopic torque
CS	1.8	Safety coefficient
σ_{yield}	$290MPa$	Strength of the selected material
RESULTS		
τ_P	$44.65Nm$	Maximum torque acting on the pendulum
τ_{Plate}	$22.33Nm$	Maximum torque acting on a single plate, half of τ_P
σ_{amm}	$161MPa$	Ratio between σ_{yield} and CS

Table 8.1: Data and results of main pendulum plate sizing.

Bibliography

[1] Matteo Melchiorre et al. "Design of a Spherical UGV for Space Exploration". In: vol. 2022-September. Cited by: 0. 2022. URL: `https : / / www . scopus . com / inward / record . uri ? eid = 2 - s2 . 0 - 85167585733 & partnerID = 40 & md5 = 7854c22969fc85ad15057fc76712b44f`.

[2] *Design and Development of a Spherical Rover for Planetary Exploration*. webpage. URL: `https://webthesis.biblio.polito.it/31455/`.

[3] Maxon Motor. *Maxon RE 40 Datasheet*. Accessed: 2024-07-10. 2022. URL: `https: //www.maxongroup.it/medias/sys_master/root/8992314425374/EN-22-159.pdf`.

[4] Maxon Motor. *GP 42 C Gearhead Datasheet*. Datasheet for Maxon GP 42 C Gearhead. 2024. URL: `https://www.maxongroup.com/medias/sys_master/root/8882781224990/EN-21-405-406-407.pdf%202021`.

[5] Maxon Motor AG. *ESCON 50/5 Servo Controller*. Datasheet. 2018. URL: `https: //www.maxongroup.ch/medias/sys_master/root/8834332459038/409510-ESCON-50-5-Manuale-di-riferimento-It.pdf`.